

See discussions, stats, and author profiles for this publication at: <https://www.researchgate.net/publication/290347989>

# Simulation of the Asian Summer Monsoon and its Dependence on Model Horizontal Resolution

Article in Journal of the Meteorological Society of Japan Ser II · April 1998

DOI: 10.2151/jmsj1965.76.2\_237

---

CITATIONS

58

READS

33

3 authors, including:



David B. Stephenson

University of Exeter

240 PUBLICATIONS 21,603 CITATIONS

[SEE PROFILE](#)



Fabrice Chauvin

CNRM-Météo-France

101 PUBLICATIONS 6,185 CITATIONS

[SEE PROFILE](#)

Some of the authors of this publication are also working on these related projects:



ReNovRisk-CYCLONES [View project](#)



The XWS open access catalogue of extreme European windstorms from 1979 to 2012 [View project](#)

## Simulation of the Asian Summer Monsoon and its Dependence on Model Horizontal Resolution

By David B. Stephenson, Fabrice Chauvin and Jean-François Royer

Météo-France CNRM, 42 Avenue Gaspard Coriolis, 31057 Toulouse Cedex, France

(Manuscript received 11 August 1997, in revised form 27 January 1998)

### Abstract

The 1986–1989 Asian summer monsoons have been simulated using a state-of-the-art atmospheric General Circulation Model (GCM), spectrally truncated at 63, 42, 31 and 21 total wavenumbers, corresponding to horizontal resolutions ranging from 200–600 km. The mean June–September Asian monsoons have been analyzed and compared to the observed mean monsoon behaviour. Large-scale features such as the lower tropospheric westerly jet, the upper tropospheric tropical easterlies, the Tibetan anticyclone, and copious rainfall over continental Asia are captured by the model at all resolutions. As the resolution is increased, the core of the low-level westerly jet moves towards Somalia and becomes more realistic. The model, however, produces excessive precipitation over the equatorial Indian Ocean and over the southern slopes of the Tibetan plateau, and these errors become accentuated at higher resolution. Furthermore, the monsoon is displaced southward at higher resolutions as is clearly evidenced by a shift in the position of the Tibetan anticyclone. A budget analysis of the upper-level vorticity suggests that this may be related to the excessive ascent over the southern slopes of the Tibetan plateau. A smooth orography test has been made at T63 truncation using T21 truncated orography, in order to assess the contribution due to orographic changes. Smooth orography alleviates the excessive precipitation over the southern slopes of the Tibetan plateau and has a strong and generally beneficial impact on the monsoon over land. It also gives large-scale dynamical monsoon indices in better agreement with observations, yet does not alleviate the excessive precipitation over the equatorial Indian Ocean. The excessive oceanic precipitation is partly due to a systematic intensification of the equatorial convergence zones with increased resolution, yet this appears to be only weakly coupled to the dynamics of the monsoon circulation.

### 1. Introduction

The Asian monsoon is the result of interactions over many differing spatial length scales from synoptic up to planetary scale. In modelling the Asian monsoon and its variability, it is important to take into account these differing scales. The optimal choice of model horizontal resolution is not evident and for this reason careful modelling studies are needed to test the sensitivity of monsoon variability to horizontal resolution. One hope is that a minimum critical resolution exists after which the monsoon is reasonably well simulated with enhanced resolution providing only finer detail, for instance near orography, but adding no new large-scale differences. The aim of this study is to examine the monsoon variability and its sensitivity to changes in

the model's horizontal resolution. A practical goal is to find the minimum horizontal resolution at which we can perform realistic monsoon simulations.

Several studies have investigated how climate simulations depend on model horizontal resolution (Boer and Lazare, 1988; Boville, 1991; Boyle, 1993; Chen and Tribbia, 1993; Gleckler and Taylor, 1993; Kiehl and Williamson, 1991; Williamson *et al.*, 1995; Giorgi and Marinucci, 1996), but only a few have specifically investigated the impact on the Asian summer monsoon. Tibaldi *et al.* (1990) discussed the behaviour of ECMWF model systematic errors in 30-day extended-range predictions made at spectral triangular truncations of T21, T42, T63, and T106. The study addressed systematic errors in the general circulation, but some results were also presented for 30-day predictions of the Asian monsoon initialised on 17 July, 1985. The main monsoon conclusions were that *the rainfall features on the scale of the subcontinent were not significantly changed at*

Corresponding author: David B. Stephenson, Météo-France CNRM, 42 Av. Gaspard Coriolis, 31057 Toulouse Cedex, France. E-mail: stephen@meteo.fr  
©1998, Meteorological Society of Japan

*higher resolution*, that T21 resolution was unable to simulate the rain shadow effect of the Western Ghats, and that there was an *erroneous northward displacement of the rainfall maximum over the west coast of India* that was present at all resolutions. Sperber *et al.* (1994) studied the Asian summer monsoon in 1-year long simulations made with the ECMWF model (cycle 33) at spectral truncations of T21, T42, T63, and T106. These climate simulations used climatological Sea-Surface Temperatures (SST) that correspond to *mean* annually-varying conditions, rather than to any particular year. They simulations proved that *T21 best captures the large-scale distribution of precipitation over the monsoon region*, although it was uncapable of capturing more regional features such as the rain-shadow in the lee of the western Ghats, and intense precipitation around the Himalayas. In the T42-106 simulations, there was a persistent rainfall maximum situated south of the equator over the Indian Ocean, which was much more apparent than in the observed precipitation climatologies. Furthermore, this *oceanic bias* became worse at higher resolution. They noted, however, that the high resolution of T106 more realistically captured the synoptic behaviour of the monsoon, for example, the Mei-yu oscillatory mode of rainfall variability over China. Lal *et al.* (1997) also noted improved realism in the monsoon onset at T106 truncation with an improved development and migration of the monsoon trough over India. Kar *et al.* (1996) noted that their T106 model better simulated the mean monsoon rainfall over western and northwestern India than did their T42 model. Sperber and Palmer (1996) compared general monsoon behaviour in 32 different General Circulation Models participating in the Atmosphere Model Intercomparison Project (AMIP), and concluded that *models with resolution  $\geq T42$  performed more poorly than lower resolution models* at capturing the monsoon rainfall correlation with ENSO, as was also noted by Kar *et al.* (1996). At much higher 50 km resolution, nested grid regional simulations of the Indian summer monsoon have produced intensified precipitation and orographically forced mesoscale circulations not originally present in the lower resolution GCM results (Bhaskaran *et al.*, 1996; and references therein).

It is not clear from these studies which horizontal resolution is optimal for simulating the monsoon and thus there is a need for further climate sensitivity experiments to address this problem. The numerical model is presented in Section 2 of this article, and is followed in Section 3 by a description of the experimental design. We have performed 7-month simulations at spectral truncations of T21, T31, T42 and T63, starting on the last day of February in 1986, 1987, 1988 and 1989. For each of the years, sea-surface temperatures have been prescribed from

observed monthly mean values and initial conditions were supplied from the ECMWF re-analysis project, which represents a best-available estimate of the actual initial state of the atmosphere and land surface. T31 truncation has been included since it may represent a good compromise between T21 and T42 resolutions, and has the advantage of being computationally cheap. The Asian monsoon possesses a rich spectrum of variability ranging from synoptic to interannual and these are all codependent and will most likely depend on resolution. However, as a first step, it is necessary to describe the mean behaviour as this is believed to be strongly related to the variability and predictability (Shukla and Fennelly, 1994; Sperber and Palmer, 1996). For example, a model which has a southward displaced mean monsoon is likely to show reduced variability in the all-India average rainfall. This study therefore focuses on the model's ability to simulate the mean Asian summer monsoon, while interesting aspects of intraseasonal, seasonal and interannual variability, which are currently under investigation, will be described in future publications. Section 4 summarises the major features of the mean Asian summer monsoon, and Section 5 presents the simulated mean Asian summer monsoons and compares them with the observations. The role played by orography is investigated in Section 6 by performing a smooth orography experiment and an analysis of the dynamical effect of the Tibetan plateau is presented in Section 7. Section 8 discusses the role played by the convergence zones and a test is made by reducing the humidity supplied to the cumulus convection parameterization. Section 9 contains a discussion and concluding remarks.

## 2. The numerical model

ARPEGE-Climat is a modular state-of-the-art spectral climate model developed from the weather forecasting model ARPEGE-IFS operationally employed at Météo-France and ECMWF. The latest version (v.2) of the model has been used, and includes some features not present in the previous versions of the model described in Déqué *et al.* (1994) and Déqué and Piedelievre (1995).

The model is a 19-level hydrostatic primitive equation model extending up to 30 km (10 hPa), using hybrid sigma-pressure levels, five of which are below 850 hPa. The horizontal fields are represented spectrally by spherical harmonics,  $\{Y_{lm}\}$ , triangularly truncated in  $(l, m)$  wave number space to give an isotropic coverage on the sphere. The collocation grid is Gaussian but is reduced at the poles in order to reduce computational redundancy associated with the convergence of the meridians. A semi-implicit Eulerian scheme is used for the advection terms.

Sub-grid scale horizontal mixing is parameterised

by  $\nabla^6$  hyper diffusion of vorticity, divergence, temperature and specific humidity. Vertical mixing is parameterised by the eddy viscosity method with Richardson number dependent exchange coefficients. A modified Charnock formula is used to calculate the surface exchange coefficients over sea thereby ensuring non-vanishing air-sea fluxes even in low wind conditions. Both deep and shallow convection are parameterised. The sub-grid scale cumulus convection parameterisation uses the Bougeault (1985) Kuo-type mass-flux scheme, and requires both low-level large-scale moisture convergence and a moist adiabatic temperature profile for convection to occur. The shallow convection uses a modified Richardson number scheme and stratiform cloudiness is calculated by comparing the humidity profile to that of a critical profile. Convective cloudiness is calculated based on the convective precipitation rate.

Prescribed sea surface temperatures are updated daily by linear interpolation of the monthly mean COLA-CAC analyses of observed sea surface temperatures (Reynolds and Smith, 1994). Surface temperature, deep soil temperatures, and surface water content are calculated prognostically by the surface scheme ISBA (Interactions between Soil, Biosphere, and Atmosphere) developed at Météo-France (Noilhan and Planton, 1989; Mahfouf *et al.*, 1995). Vertical heat transfer in the ground is based on the force-restore method, and relaxation to climatological values is no longer performed for the deep soil temperatures as was the case previously. A snow scheme is included in ISBA which takes account of ageing of the snow pack by including prognostic equations for the snow density and albedo (Douville *et al.*, 1995a,b). The scheme simulates the Eurasian snow cover realistically, with a beneficial impact on the simulation of the Asian summer monsoon (Douville *et al.*, 1995b; Douville and Royer, 1996).

The major differences between version 2 and the previous version used in the monsoon study of Royer *et al.* (1994), are a) the replacement of the two stream radiation scheme by the Morcrette scheme, b) improvements in the soil-vegetation scheme ISBA to include deep soil drainage, and prognostic thermal diffusion (deep soil temperatures no longer relaxed to a climatology), c) a more realistic snow scheme has been introduced having prognostic snow albedo and density, and d) the convection scheme has been modified slightly to increase entrainment at the cloud base (Geleyn *et al.*, 1995). The model also includes schemes for prognostic ozone evolution and convective gravity wave drag but these have not been activated for this study which is more concerned with tropospheric behaviour.

### 3. The experimental design

As part of the SHIVA project<sup>1</sup>, it was decided to focus in detail on the four summers of 1986, 1987, 1988, and 1989, which include two normal years (1986, 1989), a wet monsoon year (1988), and a dry monsoon year (1987). Summers have been simulated at four different horizontal resolutions for these years using realistic initial conditions obtained from ECMWF re-analyses for the last day of February for each year. Hence, these simulations are long-term predictions rather than being fully equilibrated climate runs, and may not have developed large systematic biases in the surface conditions often seen in multiyear climate runs. Table 1 gives information concerning model resolution, CPU time, and certain model parameters. Running T63 is almost nine times more computationally expensive than running T21, and hence it is of interest to judge what additional benefits higher resolution brings to simulating the monsoon.

It has been noted in previous studies with ARPEGE, that there is a tendency for the convergence zones to become more intense and the atmosphere to dry out with higher horizontal resolution (Déqué *et al.*, 1994; Doblas-Reyes *et al.*, 1998). A similar effect has also been noted using other models (Kiehl and Williamson, 1991; Williamson *et al.*, 1995), and is most likely a consequence of the moisture convergence closure used in the mass-flux convection scheme. As a result of this drying of the column, there is less stratiform cloudiness at higher resolution and this can modify the outgoing radiative fluxes at the top of the atmosphere by up to  $30 \text{ W m}^{-2}$  globally. To compensate for this problem, the minimum critical relative humidity used in calculating the stratiform cloudiness is routinely tuned in order to give outgoing longwave and shortwave radiation in agreement with observed climatologies. Tuning was performed empirically in this study by performing sensitivity tests for the month of March, and then choosing the parameter value that gave the outgoing radiation in closest agreement with observed satellite climatologies. The values chosen for the minimum critical relative humidity are given in Table 1, and decrease monotonically with resolution. During summer, there is much deep convection over the Asian monsoon region with most of the cloudiness being of convective origin rather than stratiform, and it is plausible that this parameter does not heavily influence the monsoon behaviour.

The adjustment of the stratiform cloudiness illustrates a fundamental problem with resolution studies — the problem of *parameter tuning*. Many of the physical parameterisations in a GCM depend

<sup>1</sup> More information concerning the SHIVA project can be found at the world wide web site <http://www.met.rdg.ac.uk/shiva/shiva.html>

Table 1. Summary information concerning the simulations. Columns are as follows: spectral truncation ( $L_{\max}$ ), number of longitudes ( $n_{lon}$ ), number of latitudes ( $n_{lat}$ ), mean grid resolution ( $Res^n$ ), model time step ( $\Delta t$ ), time to simulate 1 day using one processor of a Cray J90 (CPU), the minimum critical relative humidity for stratiform clouds ( $r_{min}$ ), and the horizontal diffusion coefficient ( $\nu$ ) in units of  $10^{25} m^6 s^{-1}$ .

$L_{\max}$	$(n_{lon} \times n_{lat})$	$Res^n$	$\Delta t$	CPU	$r_{min}$	$\nu$
T21	$64 \times 32$	$5.6^\circ$	30 min	160s	0.63	2600
T31	$96 \times 48$	$3.8^\circ$	30 min	280s	0.50	250
T42	$128 \times 64$	$2.8^\circ$	20 min	600s	0.38	40
T63	$192 \times 96$	$1.9^\circ$	15 min	1360s	0.25	3.6

strongly on model resolution and it is not at all evident which is the best way to adjust the parameters when changing model resolution. Consequently, model resolution studies are more difficult to implement and interpret than are sensitivity studies where only one external parameter is varied, such as doubled carbon dioxide experiments. A good example is afforded by the horizontal diffusion coefficient. On the basis of sensitivity tests made at ECMWF, it was decided in the resolution studies of Tibaldi *et al.* (1990) and Sperber *et al.* (1994), to use half the horizontal biharmonic ( $\nu \nabla^4$ ) diffusion coefficient ( $\nu$ ) at T106 resolution compared to that used at lower resolutions. In Sperber *et al.* (1994), it was found that the mean July 850 hPa wind speed in the Somali jet and over the northern equatorial Indian Ocean weakened with resolution, T21 → T63, and then regained some strength at T106 resolution. Stephenson (1994) demonstrated that the energy budget can be sensitive to the choice of the horizontal diffusion coefficient, even at resolutions as high as T42, and it is not impossible that the inertial low-level Somali jet in Sperber *et al.* (1994), regained some strength due to the weakened diffusion coefficient used at T106. In the ARPEGE model, a more scale-selective higher order horizontal diffusion (hyperviscosity) coefficient ( $\nu \nabla^6$ ) is used where the e-folding time for the highest spherical harmonic is fixed at 8.3 hours, regardless of model resolution, causing the diffusion coefficient to scale as  $\nu \sim L_{\max}^{-6}$  with model truncation  $L_{\max}$  (values for  $\nu$  are given in Table 1).

For each year, the simulations were started on 12Z of the last day of February, taking into account the leap year in 1988, and ran until the last day of September. The atmosphere was initialized for each of the years using 31-level T106 analyses obtained from the re-analysis project at ECMWF (Gibson *et al.*, 1994). The same analysis was used for all the different horizontal resolutions and the analyses were linearly interpolated onto the model grid. The lower boundary fields such as surface temperature, surface water content and snow depth were also initialized using the ECMWF re-analyses. The sur-

face temperature was vertically extrapolated onto the model orography assuming a standard lapse rate of 6.5 K/km, whereas no extrapolation was used for the other surface fields. The initialized surface water content was slightly modified to be compatible with the soil textural properties and vegetation parameterisation in ISBA. It was also necessary to initialize some variables not available in the re-analyses: initial snow albedo was set to 0.7 and initial snow density was set to 300 kg/m<sup>3</sup>. The initial surface boundary conditions are those assimilated into the ECMWF model for the last day of February of each year. Whilst these are consistent with the initial atmospheric state, it is possible that the re-analysed surface fields, such as snow depth, are strongly model dependent and may contain systematic errors (Dr. Franco Molteni, personal communication). Optimal interpolation analyses (Reynolds and Smith, 1994) of observed sea-surface temperatures were used both as initial conditions and were prescribed throughout the simulations, as was also the case for the ECMWF re-analyses.

#### 4. Observed asian summer monsoon

The life cycle of the Asian summer monsoon commences with an abrupt onset in spring, followed by an active period in June–August bringing much rain to Asia, and then slowly dies out over autumn. To summarise its behaviour during its active phase, summertime means, obtained by averaging over the 4 months (122 days) June–September (JJAS) will be presented. June–August (JJA) averages have also been made (not shown) and agree well with the JJAS ones presented following. However, to improve statistical analysis it was decided to present results obtained over the longer averaging period, as was also done in Sperber and Palmer (1996). The results will be presented for the latitudinal domain 20°S–40°N and longitudinally from 30–150°E. The extended longitudinal domain allows one to examine the behaviour in the convective region of the warm pool in the western Pacific, from where many of the convective monsoon systems originate. A contracted description of the observed mean monsoon is given

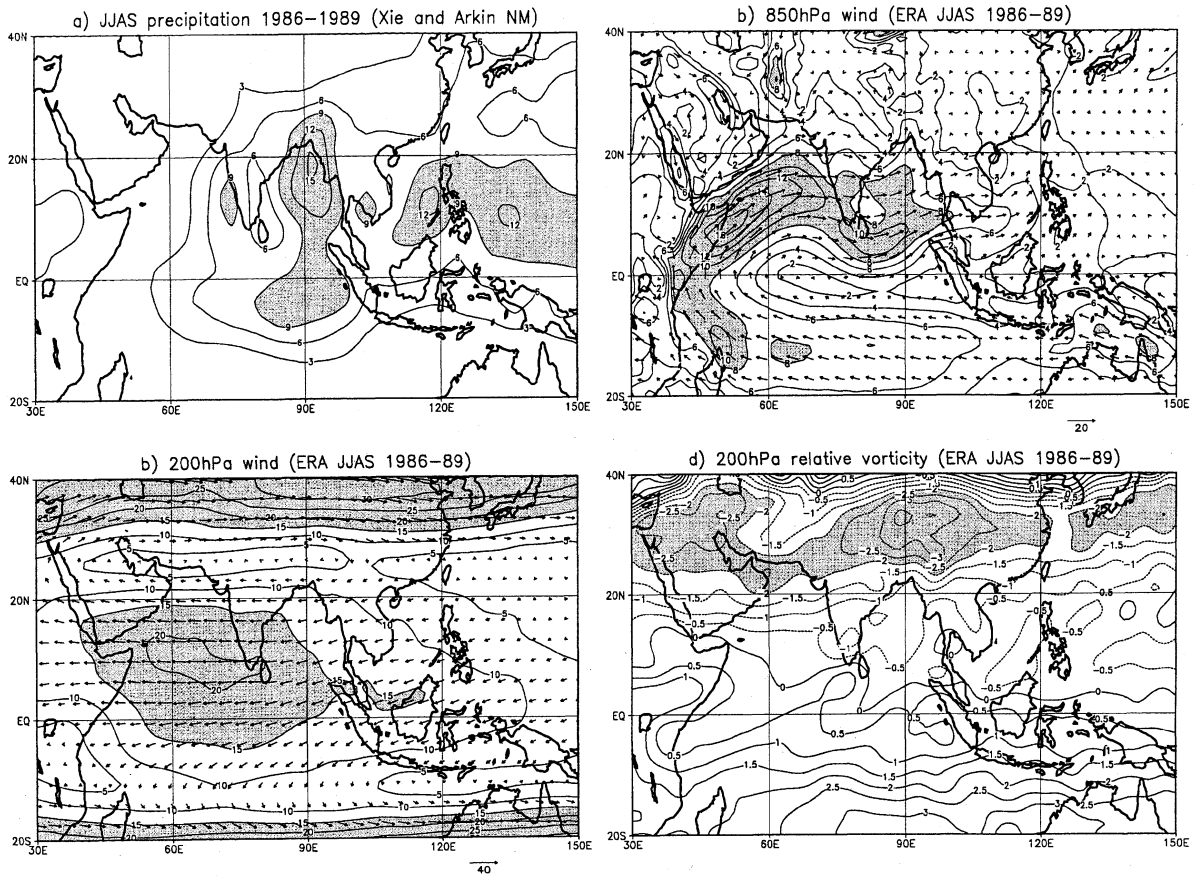


Fig. 1. The mean observed summer monsoon (JJAS) for 1986–1989. a) Mean precipitation rates from the merged analyses of rain-gauge and satellite-based observations (Xie and Arkin, 1996) (contours every 3 mm/day with values above 9 mm/day shaded), b) the mean ECMWF re-analysed 850 hPa velocity vectors ( $u, v$ ) and isotachs (every 2 m/s,  $> 8$  m/s shaded), c) the mean ECMWF re-analysed 200 hPa velocity vectors ( $u, v$ ) and isotachs (every 5 m/s,  $> 15$  m/s shaded), and d) the mean relative vorticity at 200 hPa obtained from the ECMWF 200 hPa winds (contours every  $0.5 \times 10^{-6} \text{ s}^{-1}$ , and anticyclonic values less than  $-2 \times 10^{-6} \text{ s}^{-1}$  shaded).

by the fields presented in Fig. 1.

#### 4.1 Rainfall

Figure 1a shows the mean 1986–89 June–September precipitation rate obtained for the Climate Prediction Center (CPC) Merged Analysis of Precipitation (CMAP) data, which combines both gauge observations and satellite-derived estimates (Xie and Arkin, 1996). The mean precipitation exceeds 6 mm/day over the broad region of South East Asia, with local maxima occurring over the ocean west of India, the northern part of the Bay of Bengal, and over the south equatorial Indian Ocean region 70–100°E. The maximum over the Phillipines is the westward extension of the Inter-Tropical Convergence Zone, which lies north of the equator in summertime. Means (not shown) have also been made using merged analyses including NCEP model predictions (Xie and Arkin, 1996), and were found to closely resemble those shown in Fig. 1a without model input, suggesting that satellite and rain gauge

data coverage was adequate over the Asian monsoon and Indian Ocean regions.

The maximum precipitation associated with the cyclonic convergence zone over the south equatorial Indian Ocean (70–100°E, EQ–10°S) is extremely marked in Fig. 1a and represents a substantial quantity of summertime rainfall. It is apparent to a lesser extent in other precipitation climatologies such as that of Legates and Willmott (1990), and in cloudiness estimates derived from satellite measurements of outgoing longwave radiation. In the CMAP data, rainfall measurements from about 100 atoll gauges over the Western Pacific (the Morrissey data set) were used to calibrate the amplitude of the satellite-derived oceanic precipitation for the whole of the tropics, and no data was included from gauge measurements made on atolls in the Indian Ocean. Although there are no islands situated in the vicinity of maximum precipitation around (90°E, 5°S), there are islands in the Chagos archipelago, in the western

edge of the zone. Notably, there is the coral atoll, Diego Garcia, at (72.4°E, 7.2°S), which receives an average of 6.3 mm/day in the dry season (JJAS), resulting from fast-moving light rain showers associated with the predominant south-easterly flow. Climatological estimates from the merged analyses for 1979–95 give JJAS mean values of 6–7 mm/day for this region consistent with the independent ground based measurement of 6.3 mm/day obtained for Diego Garcia. This simple validation gives some confidence in the satellite derived estimates of the rainfall over the equatorial Indian Ocean. The measurements made at Diego Garcia might also be useful in future studies of monsoon variability.

It should be noted that in the climatology presented in Fig. 1a, there is no evidence of enhanced rainfall over the Himalayas or its foothills. Gauge-corrected climatologies such as those done by Legates and Willmott (1990) and Hulme (1992) show a narrow intense Himalayan band of rainfall with values around 10 mm/day, yet this feature is absent in the CMAP climatology which uses uncorrected rain gauge estimates. Rainfall estimates in mountainous regions such as Nepal are known to exhibit strong spatial heterogeneities (Pant and Kumar, 1997), and therefore extreme care should be exercised when making and interpreting gridded climatologies in such regions. Roughly speaking, the CMAP climatology appears to underestimate precipitation over orography, yet has larger estimates over the equatorial Indian ocean compared to the Legates and Willmott (1990) climatology. The large differences between observed precipitation climatologies should not be forgotten when judging the quality of simulated monsoon rainfall patterns.

#### 4.2 Lower tropospheric flow

Figure 1b shows the JJAS summertime lower troposphere 850 hPa flow obtained from ECMWF re-analyses for the period 1986–89. There is a strong mean cross-equatorial flow towards Asia which veers to the east due to the influence of orographic barriers such as the East African highlands, and due to the Coriolis effect which acts so as to conserve absolute planetary vorticity (Rodwell and Hoskins, 1995). The flow becomes concentrated into a strong low-level jet over the flat eastern areas of Kenya and the Somali coast, resulting in strong peak wind speeds of up to 100 knots (51.5 m/s), first reported by Royal Air Force pilots and navigators (Findlater, 1969). The JJAS mean wind speed in the core of the Somali/Findlater jet is 17–18 m/s and the core is centered at (53°E, 9°N) off the coast of northern Somalia, and causes cool coastal waters to up-well to the surface. Strong westerlies traverse the southern and central parts of India before becoming south westerlies which impinge the west coasts of Burma and Thailand. Strong southward and south-

eastward flows are present over Persia and the Arabian peninsula and bring warm dry air into northwest India (Sperber and Palmer, 1996). Broadly speaking there is a band of positive cyclonic vorticity centered on 20°N (not shown), associated with the monsoon trough, and a band of negative vorticity to the south of it over the equatorial Indian Ocean. Negative vorticity gives rise to cyclonic circulation south of the equator and this is associated with the maximum of precipitation over the south equatorial Indian Ocean. On the southeastern flank of the Somali jet, there is a minimum in relative vorticity of  $-2.5 \times 10^{-5} \text{ s}^{-1}$ , having a similar magnitude to the local background planetary vorticity.

#### 4.3 Upper tropospheric flow

Figure 1c shows the JJAS summertime upper troposphere 200 hPa flow obtained by averaging the ECMWF re-analyses over the period 1986–89. Strong easterly flow exists over the Indian Ocean with maximum values at 10°N exceeding 20 m/s. Comparison with the low level flow in Fig. 1b, reveals that a) the upper level flow is in general stronger than the lower level flow, and b) is in the opposite direction to the lower level tropical westerly flow. This strong vertical shear over the Indian Ocean is due to the existence of strong divergent circulation, and can be used as to define a dynamical index for the large-scale monsoon. More will be said about this later in this article. The northern hemisphere sub-tropical westerly jet is centered around 40°N at 200 hPa and is north of the Tibetan plateau. Between the westerly and easterly jets, there is a strong meridional shear in the zonal wind and this gives rise to the Tibetan anticyclone clearly visible as a minimum in the relative vorticity (Fig. 1d), centered on (90°E, 33°N). A small scale north-south dipole can also be seen in the relative vorticity at the southern tip of India and is due to the generation of anticyclonic vorticity by air parcels contracting as they pass over the Western Ghats.

### 5. Modelled asian summer monsoon

#### 5.1 Simulated Rainfall

Figure 2 shows the JJAS mean precipitation rate calculated from the model results at different horizontal resolutions. Compared to the CMAP observations (Fig. 1a), it can be seen that the mean precipitation is too strong in the model, even at the lowest resolution (T21). A large band of maximum mean precipitation is centered over Thailand and the Phillipines and extends westwards over India and southeastwards to join the ITCZ over the northern equatorial Pacific. At higher resolution, the band is displaced southwards becoming more aligned with the Pacific ITCZ at 5–10°N, which intensifies.

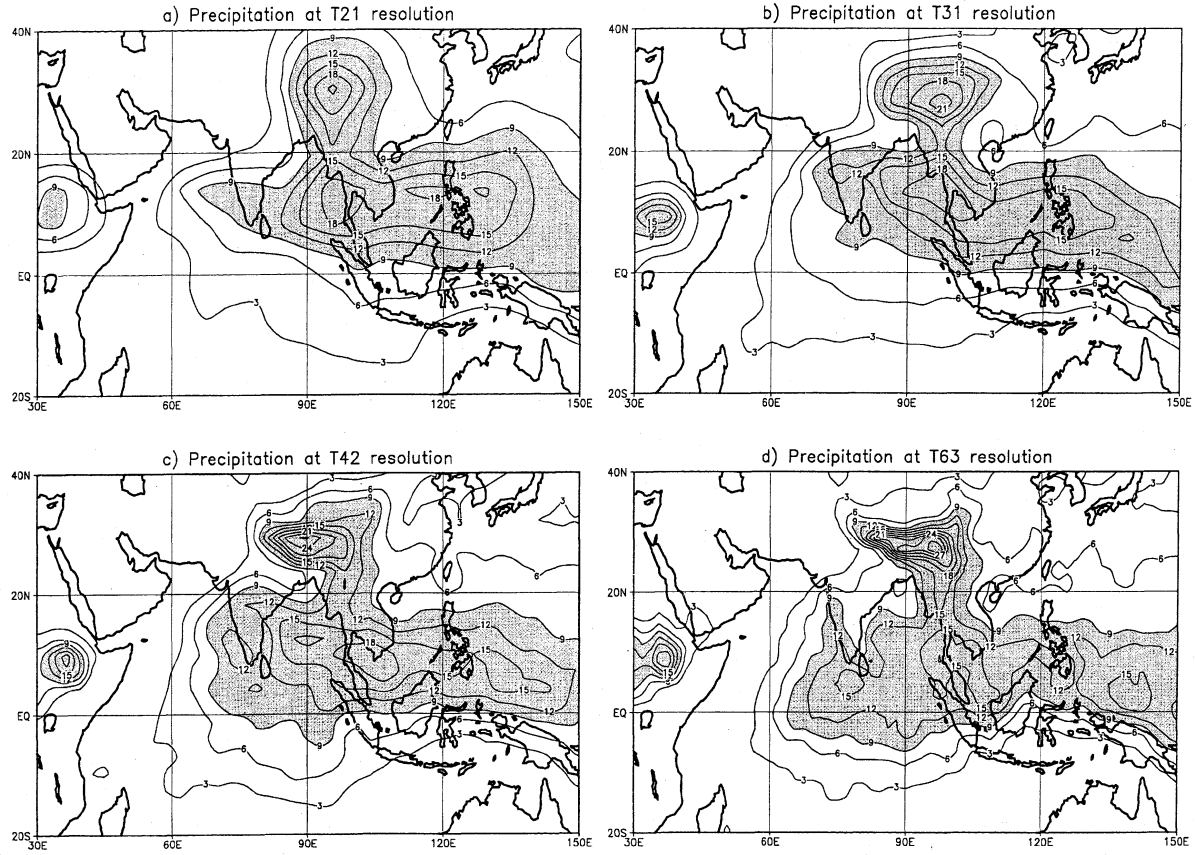


Fig. 2. Mean summertime (JJAS) precipitation rates averaged over 1986–89 from the model simulations made at a) T21, b) T31, c) T42, and d) T63 spectral truncations. Contours every 3 mm/day with values above 9 mm/day shaded.

In addition to using geographic maps to examine the qualitative spatial distribution of the rainfall, it is useful to make averages over selected regions in order to quantify the changes. Table 2 presents the mean JJAS rainfall for both model and observations averaged over four different rectangular latitude-longitude regions. There exists an arbitrariness in choosing the averaging regions and the choice can be particularly delicate with such a spatially variable field as precipitation. The EXT and IND regions follow the definitions proposed by Goswami (personal communication) (1997) with the exception that our regions extend only to  $25^{\circ}\text{N}$  and not  $30^{\circ}\text{N}$ , so as not to include the excessive orographic precipitation in the model. They aim at summarizing the mean rainfall over India and South East Asia (EXT) and over India (IND), and include both land and sea regions. The IND values are slightly larger than values obtained for the land average 1986–1989 JJAS all-India rainfall ( $7 \pm 1 \text{ mm/day}$ ), as to be expected due to the inclusion of adjacent coastal regions which experience heavy precipitation. The EQU region summarizes the mean rainfall over the equatorial Indian Ocean region, and the HIM region summarizes the rainfall over the southern slopes of the Himalayas

and the Tibetan plateau. Values are also included for the sensitivity tests, T63s and T63t, which will be discussed later in this article.

All experiments have more precipitation than observed in the EXTended and HIMalayan regions, and all but the lowest resolution also overestimate the precipitation in the EQU region. At T21 resolution, the rainfall maximum is displaced too far eastwards causing too little rain in the IND region but too much in general in the EXT region. At higher resolution the ratio of IND precipitation to EXT precipitation improves up until T63 resolution where the precipitation moves south of India over the EQU region. There is a monotonic tendency for the precipitation to increase over the EQU region with increasing model resolution, giving unrealistic amounts in this region.

The HIM precipitation increases monotonically with resolution up until T63 where it starts to reduce, due most likely to the clear southward shift evident at this resolution. Examination of Fig. 2 reveals that as the resolution increases the orographic rainfall becomes concentrated into a narrower region yet the mean HIM amount stays roughly constant. Excessive amounts of precipitation occur over the

Table 2. Mean June–September precipitation rates (mm/day) averaged over different monsoon regions: EXTended monsoon region ( $70\text{--}120^\circ E, 10\text{--}25^\circ N$ ), EQUatorial region ( $70\text{--}120^\circ E, 7.5^\circ S\text{--}7.5^\circ N$ ), INDian region ( $70\text{--}95^\circ E, 10\text{--}25^\circ N$ ), and HIMalayan region ( $75\text{--}105^\circ E, 25\text{--}35^\circ N$ ). Climatological rainfall rates for the rainfall dataset of Legates and Willmott (1990) are also presented, together with 1986–89 mean observed CMAP values (Xie and Arkin, 1997) and their standard errors. Simulated values lying within two standard errors of the mean CMAP values are marked in bold face. The last two columns give ratios of average precipitation rates expressed in per cent.

Source	EXT	EQU	IND	HIM	EQU/EXT	IND/EXT
T21	11.1	<b>7.1</b>	<b>8.6</b>	10.5	64 %	77 %
T31	11.4	<b>8.3</b>	10.9	11.7	73 %	96 %
T42	11.0	9.7	<b>10.6</b>	12.5	88 %	96 %
T63	<b>9.7</b>	10.7	<b>8.8</b>	11.8	111 %	90 %
T63s	<b>9.5</b>	10.5	<b>8.2</b>	6.6	110 %	86 %
T63t	10.7	9.8	<b>10.4</b>	11.8	92 %	97 %
L&W	9.9	<b>6.5</b>	<b>9.9</b>	6.1	66 %	100 %
CMAP	<b><math>8.7 \pm 0.5</math></b>	<b><math>7.7 \pm 0.9</math></b>	<b><math>9.2 \pm 0.8</math></b>	<b><math>4.4 \pm 0.4</math></b>	89 %	106 %

steepest slopes of the Himalayas and Eastern Tibet ( $> 25$  mm/day) and this feature is not present in the merged analyses shown in Fig. 1a. This is most likely a model systematic error due to the way in which the atmospheric flow is calculated over steep orography. Other spectral GCMs also tend to overestimate the mean rainfall in this region (Sperber *et al.*, 1994; Ju and Slingo, 1995; Dong *et al.*, 1996; and most versions of the ECMWF operational forecasting model). This systematic error also used to be present in the UKMO grid point model (Gadgil *et al.*, 1998) but is less evident in the current version of the model (Dr. Gill Martin and Dr. Roy Kershaw, personal communication). The precipitation maximum over the north of the Bay of Bengal is missing from the simulated precipitations especially at higher resolutions and this could be due to convection being suppressed in this region by subsiding air coming from the excessive convection over the Tibetan slopes and from over the equatorial Indian Ocean.

In the observed precipitation (Fig. 1a), a local rain-shadow effect occurs in the lee to the east of the western Ghats. This only starts to appear in the model results at T63 resolution, whereas in Sperber *et al.* (1994) it was apparent even at T42 resolution — this is due to the representation of the Ghats in our model which will be discussed in more detail in section 6.

### 5.2 Simulated lower tropospheric flow

Figure 3 shows the 850 hPa wind averaged over the four summers from 1986–89 for the model results. All resolutions show a marked zonally oriented westerly jet traversing India as seen in the analyses in Fig. 1b. The jet is well-situated over India, not too far north as in the studies of Tibaldi *et al.* (1990) and Sperber *et al.* (1994), where it was speculated that this might be due to the ECMWF

model (at that time) having no gustiness correction for air-sea fluxes at low wind speed. Maximum wind speeds in the core of the jet are between 17–18 m/s for all model resolutions, and no systematic weakening (Tibaldi *et al.*, 1990) or strengthening (Kar *et al.*, 1996) is seen with increasing resolution. However, the core of maximum wind speed in the jet is strongly displaced eastwards downstream at low resolution and moves towards Somalia at higher resolutions — T21 ( $76^\circ E, 13^\circ N$ ), T31 ( $60^\circ E, 13^\circ N$ ), T42 ( $57^\circ E, 12^\circ N$ ), and T63 ( $52^\circ E, 11^\circ N$ ). Furthermore, at low resolution the westerly jet penetrates too far eastward over Southeast Asia and this systematic error is reduced at the highest resolution (T63). This behaviour can also be seen in the results of the T42 and T106 simulations of Kar *et al.* (1996) (their Fig. 1). An associated westward contraction with increasing resolution also occurs in the monsoon trough (minimum in sea-level pressure — not shown), and this is perhaps due to the more intense monsoon low pressure systems at high resolution penetrating further westwards into the Indian subcontinent. Examination of 850 hPa relative vorticity (not shown) reveals that at T21 resolution, the flow is too zonally symmetric compared to that of the ECMWF analyses, suggesting a poor representation of stationary waves in the Asian region. At T31 this problem ameliorates significantly and distinct cyclonic vorticity maxima become apparent over the Bay of Bengal and the Arabian peninsula.

### 5.3 Simulated upper tropospheric flow

Figure 4 shows the 200 hPa wind averaged over the four summers from 1986–89 for the model results. All resolutions show a strong easterly flow over the Indian Ocean. At T21 and T31 resolution, the maximum easterly flow is situated too far northeast as is the minimum in wind speed over Tibet. At higher resolution, the maximum easterlies occur

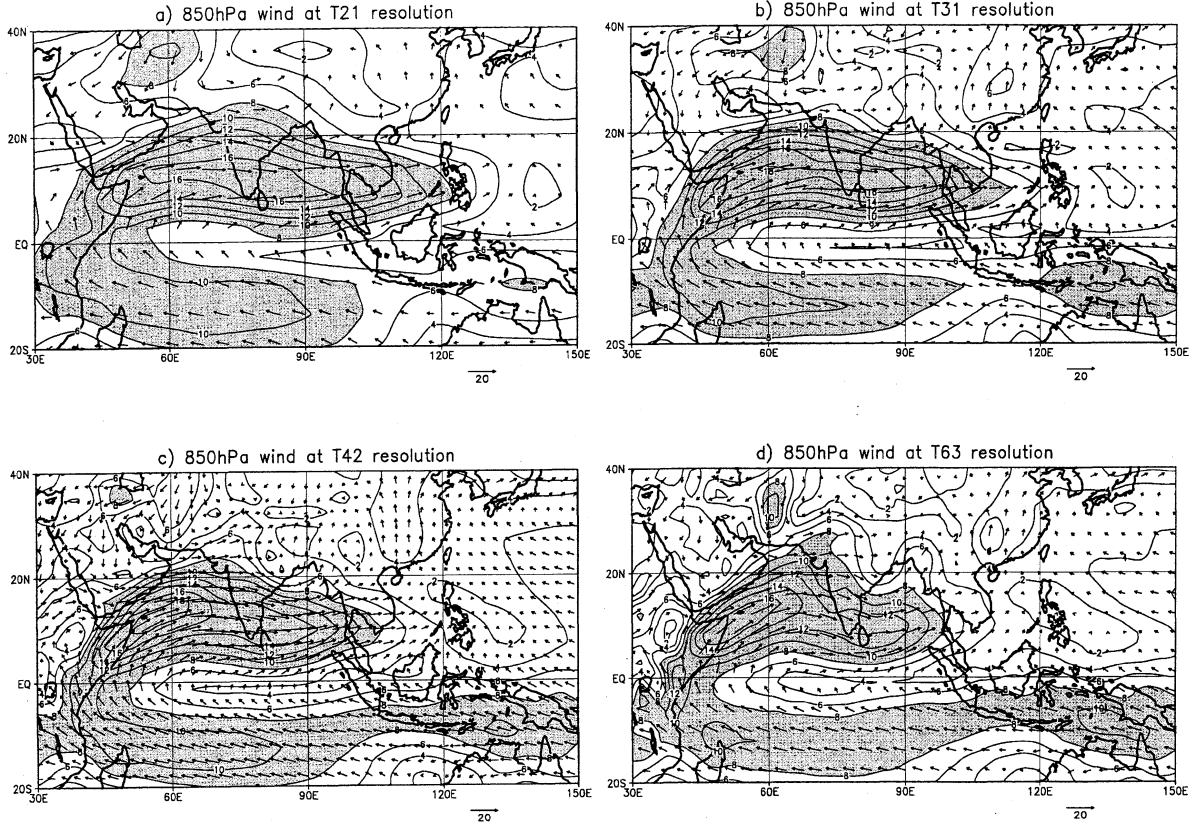


Fig. 3. Mean summertime (JJAS) 850 hPa wind vectors and isotachs averaged over 1986–89 from the model simulations made at a) T21, b) T31, c) T42, and d) T63 spectral truncations. Isotachs every 2 m/s and wind speeds exceeding 8 m/s shaded.

further south giving a more realistic flow pattern over Asia. However, the winds are stronger than in the analyses (Fig. 1c), especially the southward flow over China which then crosses the equator. This suggests that the model has an excessively intense transport of upper level mass towards the Southern Hemisphere and hence an excessive monsoon meridional overturning circulation consistent with the simulated mean precipitation being too strong.

Figure 5 shows the relative vorticity calculated from the 200 hPa winds shown in Fig. 4. The Tibetan anticyclone (minimum in vorticity) is visible over Asia (grey shaded) but is too far north at T21 and T31 resolutions when compared to that of the ECMWF analyses (Fig. 1d). Furthermore, the relative vorticity minimum is weaker than that of the observations at all resolutions and does not extend eastward over the Pacific ocean, especially at T63 resolution. At T42 and T63 resolutions, there is a strong vorticity gradient over China associated with the intense southward flow visible in Fig. 4d. At T63, the zero vorticity isoline starts to resemble that of the observations over the tip of India, suggesting that the atmosphere is starting to respond to the western Ghats, as was also noted in the rain shadow visible in the mean precipitation.

#### 5.4 Vertical wind shear

From simple steady state models of the tropical atmosphere, it is expected that strong heating in the tropics will give rise to strong vertical shears in the horizontal flow (Gill 1980). By looking at the vertical shears rather than particular levels, one projects more onto the baroclinic modes that are forced by the divergent circulation and hence one can get some insight into the large-scale divergent circulation. Webster and Yang (1992) proposed that the zonal wind shear,  $u_{850} - u_{200}$ , averaged over the domain ( $40\text{--}110^\circ\text{E}$ ,  $\text{EQ}\text{--}20^\circ\text{N}$ ), would provide a good index of the large-scale monsoon circulation (hereafter referred to as the U-index). It has been used in various modelling studies of the monsoon (Ju and Slingo, 1995; Kitoh *et al.*, 1997) and correlates better with ENSO than do rainfall indices of the monsoon. There is, however, *almost zero correlation* between the zonal wind shear index and the interannual variations in all-India rainfall (Webster and Yang, 1992). Furthermore, in the doubled CO<sub>2</sub> experiment of Kitoh *et al.* (1997) it was noted that while the monsoon precipitation significantly increased with global warming, the wind shear index actually decreased. Goswami (personal communication) has argued that the U-index detects

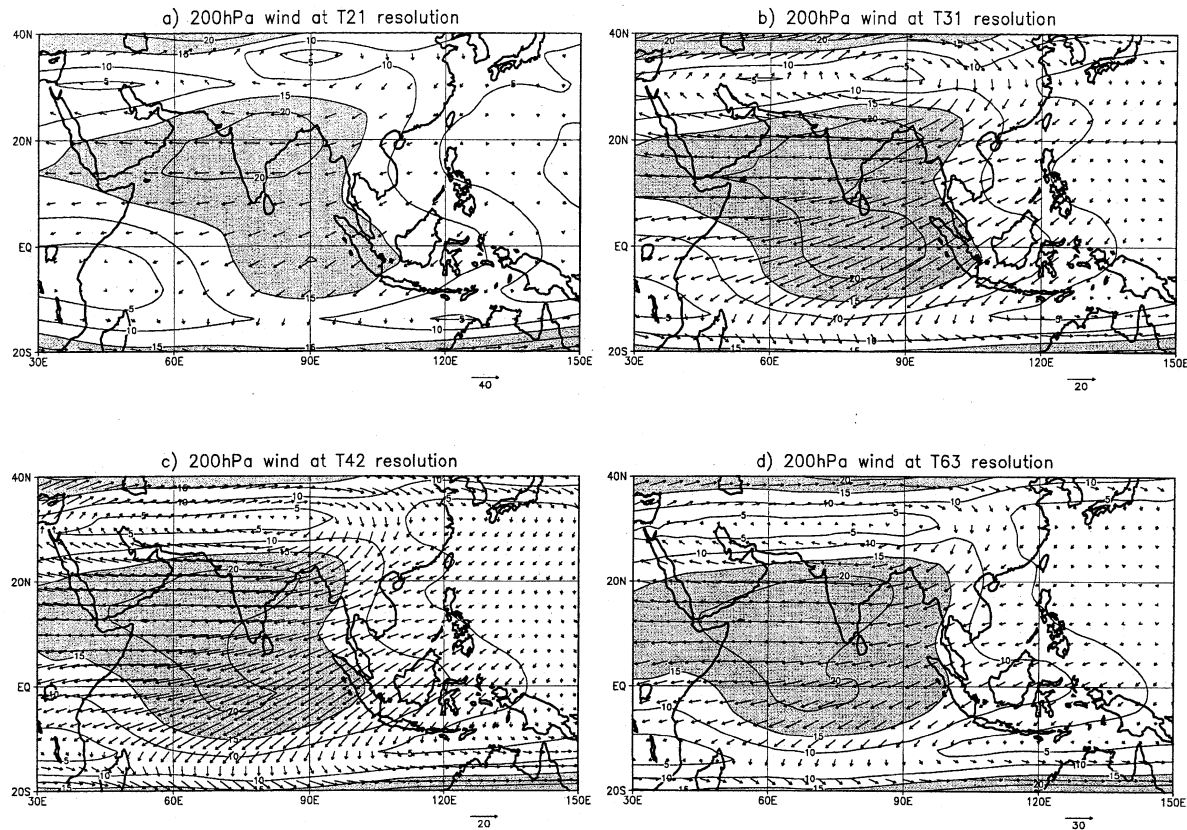


Fig. 4. Mean summertime (JJAS) 200 hPa wind vectors and isotachs averaged over 1986–89 from the model simulations made at a) T21, b) T31, c) T42, and d) T63 spectral truncations. Isotachs every 5 m/s and wind speeds exceeding 15 m/s shaded.

the equatorial longitudinal circulation rather than detecting the local Hadley circulation which transports air meridionally northward over Asia at low levels and southward at upper levels. An early draft of Goswami's proposed a monsoon V-index based on the vertical shear of the meridional wind averaged over (40–140°E, 15S–25°N). Goswami *et al.* (1997) later discovered that, for interannual variations, it is better to define the V-index over the smaller region of (70–110°E, 10–30°N). The original larger-scale V-index has been adopted in this study for comparing the mean monsoon behaviours.

Table 3 presents both the U-index and the V-index (the area average of  $v_{850} - v_{200}$ ) together with the 200 hPa contribution. Both the U- and V-indices simulated by the model are too strong compared to the ECMWF and NCEP re-analyses, and suggest that the simulated monsoon is too strong, in agreement with the excessive simulated precipitation rates (Table 2). The 1986–89 mean NCEP indices are within 2 standard errors of the mean ECMWF indices, yet it is of interest to note that the NCEP U-index is larger than the ECMWF U-index yet has smaller interannual variations in the period 1986–89. The simulated U- and V-indices decrease with increasing resolution towards more real-

istic values, with the most realistic values being obtained for the smooth orography experiment T63s. More than 70 % of the observed U-index is due to the 200 hPa component and the model tends to give lower percentages, especially at lower resolution, due to the excessive extension of the 850 hPa westerly jet over South East Asia. The upper level contribution to the U-index is within two standard errors of the value from the ECMWF re-analyses, implying that the overestimation of the U-index is mainly due to excessive low-level flow. The upper level contribution to the U-index is a measure of the strength of the upper tropospheric tropical easterly jet and tends to be larger than in the ECMWF analyses particularly at higher resolutions. Kar *et al.* (1996) also found that the tropical easterly jet strength was larger than observed but moreso at T42 than at T106 resolution. It should be noted that the V-index shows a much larger fractional change in going from T21 to T63 than does the U-index, and is therefore a more sensitive indicator of the large-scale monsoon dynamics.

### 5.5 Summary

It is instructive to examine the differences between the T63 and the T21 simulations (interpo-

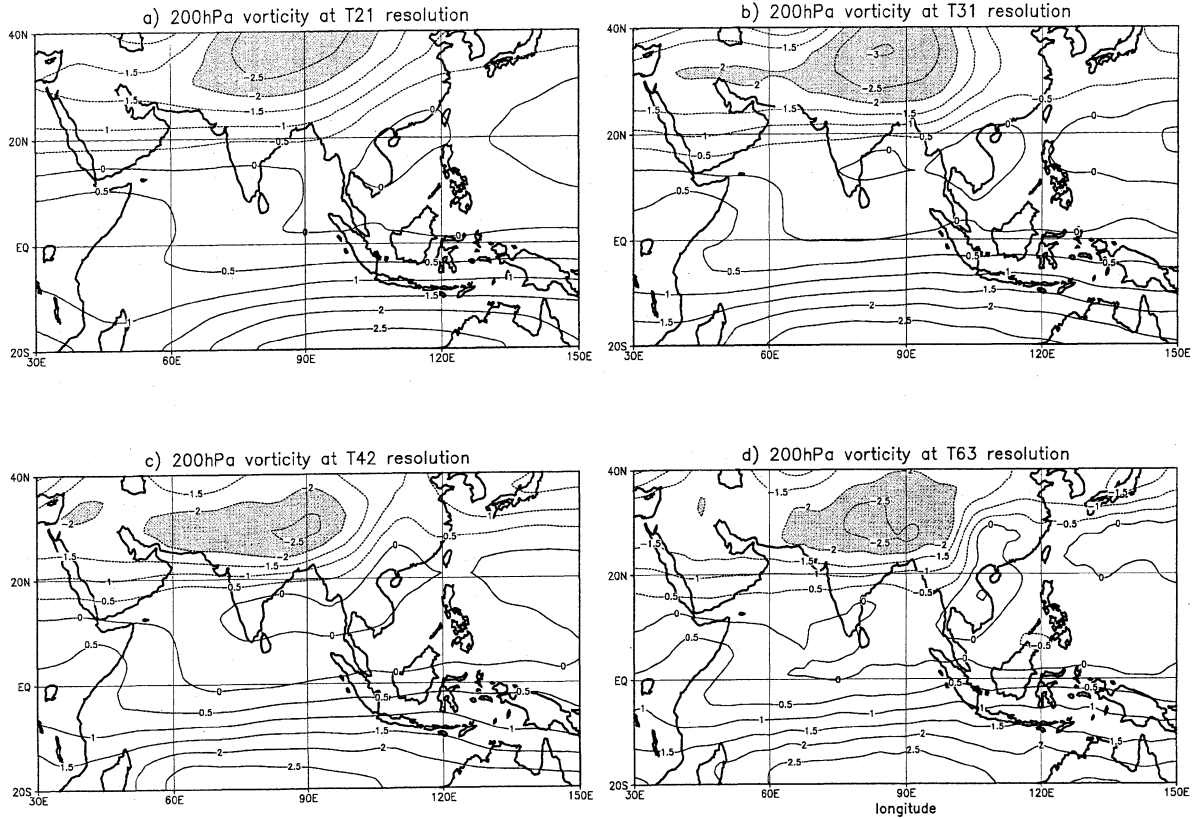


Fig. 5. Mean summertime (JJAS) 200 hPa relative vorticity averaged over 1986–89 from the model simulations made at a) T21, b) T31, c) T42, and d) T63 spectral truncations. Contours every  $0.5 \times 10^{-6} \text{ s}^{-1}$ , and anticyclonic values less than  $-2 \times 10^{-6} \text{ s}^{-1}$  shaded.

Table 3. Mean June-September wind shear indices and upper level components in m/s. The U-index follows Webster and Yang (1992) and is defined over the domain ( $40\text{--}110^\circ\text{E}$ ,  $\text{EQ}\text{--}20^\circ\text{N}$ ). The V-index follows Goswami et al. (1997) and is defined over the domain ( $40\text{--}140^\circ\text{E}$ ,  $15^\circ\text{S}\text{--}25^\circ\text{N}$ ). Both NCEP and ECMWF reanalysis estimates for 1986–89 are given, and figures in bold face denote simulated values lying within two standard errors of the mean ECMWF value (95 % confidence limits). The percentages contribution of the upper level 200 hPa winds to the indices are also quoted.

Model	U-index	$U_{200}$	% $U_{200}$	V-index	$V_{200}$	% $V_{200}$
T21	26.7	<b>-15.8</b>	59 %	7.2	-4.5	62 %
T31	27.5	<b>-17.4</b>	63 %	7.0	-4.4	63 %
T42	26.5	<b>-17.1</b>	65 %	6.7	-4.1	61 %
T63	25.8	<b>-18.0</b>	70 %	6.2	<b>-3.6</b>	58 %
T63s	<b>22.3</b>	<b>-14.7</b>	66 %	<b>5.5</b>	<b>-3.2</b>	58 %
T63t	25.7	<b>-17.0</b>	66 %	6.3	<b>-3.7</b>	59 %
NCEP	$23.4 \pm 1.3$	$-17.3 \pm 1.2$	74 %	$4.7 \pm 0.1$	$-3.3 \pm 0.2$	70 %
ECMWF	$21.9 \pm 1.7$	$-15.8 \pm 1.3$	72 %	$4.8 \pm 0.5$	$-2.8 \pm 0.4$	59 %

lated onto the T63 Gaussian grid) shown in Fig. 6, which summarize the resolution changes. Compared to T21 resolution, T63 resolution gives an excess of precipitation over the southern slopes of the Tibetan plateau, over the equatorial Indian Ocean, and over northern India (Fig. 6a). There are deficits of precipitation north of the Himalayas and over South East Asia and the Phillipines.

It should be noted that the magnitude of the T63-T21 precipitation changes exceed those obtained from natural interannual variability. Typical changes are of the order of 5 mm/day compared to interannual standard errors of around 3 mm/day (not shown). A simple, yet not the most reliable, way to test the significance of the precipitation anomalies is to calculate the ratio of the changes

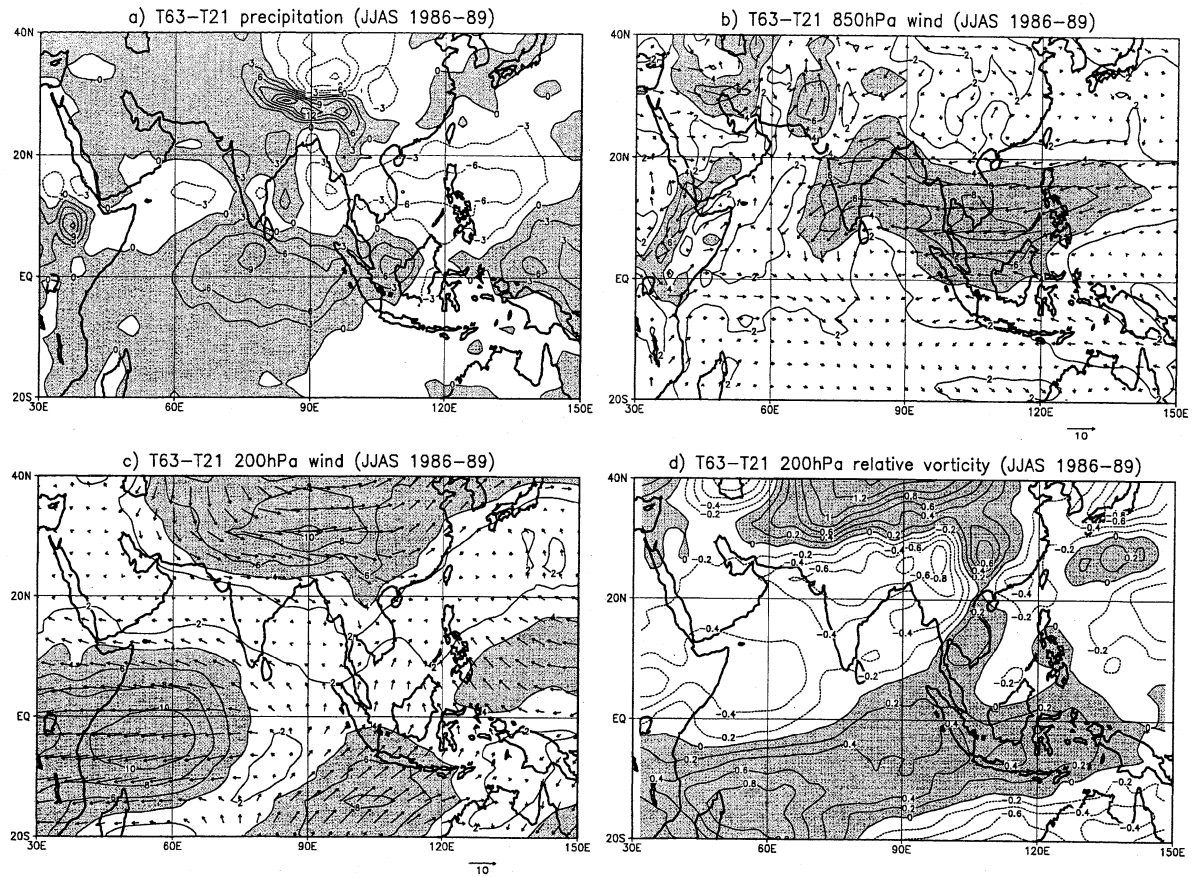


Fig. 6. Mean difference between T63 and T21 summer monsoons (T63-T21): a) Mean precipitation rates (contours every 3 mm/day with positive values shaded), b) 850 hPa velocity vectors ( $u, v$ ) and isotachs (every 2 m/s,  $> 4$  m/s shaded), c) 200 hPa velocity vectors ( $u, v$ ) and isotachs (every 2 m/s,  $> 4$  m/s shaded), and d) the 200 hPa relative vorticity at 200 hPa (contours every  $0.2 \times 10^{-6} \text{ s}^{-1}$ , and positive differences shaded).

divided by the interannual standard errors, which is expected to be Student-t distributed if the changes are due solely to sampling (Zwiers, 1994). Maps of t-values have been made (not shown) and have typical values exceeding 2.5, which suggests that the changes are not the result of sampling errors at 95 % confidence. Additional confirmation that the changes are not merely the result of sampling errors is also suggested by the very similar precipitation pattern obtained in the T106-T42 difference presented in Fig. 5c of Kar *et al.* (1996), despite their equatorial increase being located slightly further south.

The low level wind changes (Fig. 6b) clearly show the reduction in the excessive eastward extension of the low level westerly jet. The deceleration of the westerly jet over South East Asia gives rise to mean low level convergence to the west of India and over the Bay of Bengal. At lower resolution, the jet extends further eastwards and hence the low-level convergence regions are displaced eastwards toward the Phillipines. In Fig. 6b, a region of increased

low-level convergence can be seen as the difference wind field curves towards the equator around 70E—consistent with increased equatorial precipitation at higher resolutions. The upper level wind differences (Fig. 6c) show an increased easterly flow over the western equatorial Indian Ocean. Over the Tibetan region, the upper level winds become more westerly at higher resolution related to the southward shift in the Tibetan anticyclone, evidenced by the north-south dipole in the relative vorticity in Fig. 6d.

The mean precipitation over the EXT monsoon region of India and Southeast Asia, and the dynamical wind shear U- and V-indices suggest that the monsoon weakens at higher resolution, becoming more in agreement with the observed broad-scale behaviour. However, there is also a tendency at higher resolutions for the precipitation to increase over the equatorial Indian Ocean and the southern slopes of the Tibetan plateau and this makes the simulations less realistic. At lower resolutions, the Tibetan anticyclone is situated too far north as are the precipitation and the low-level winds, and these

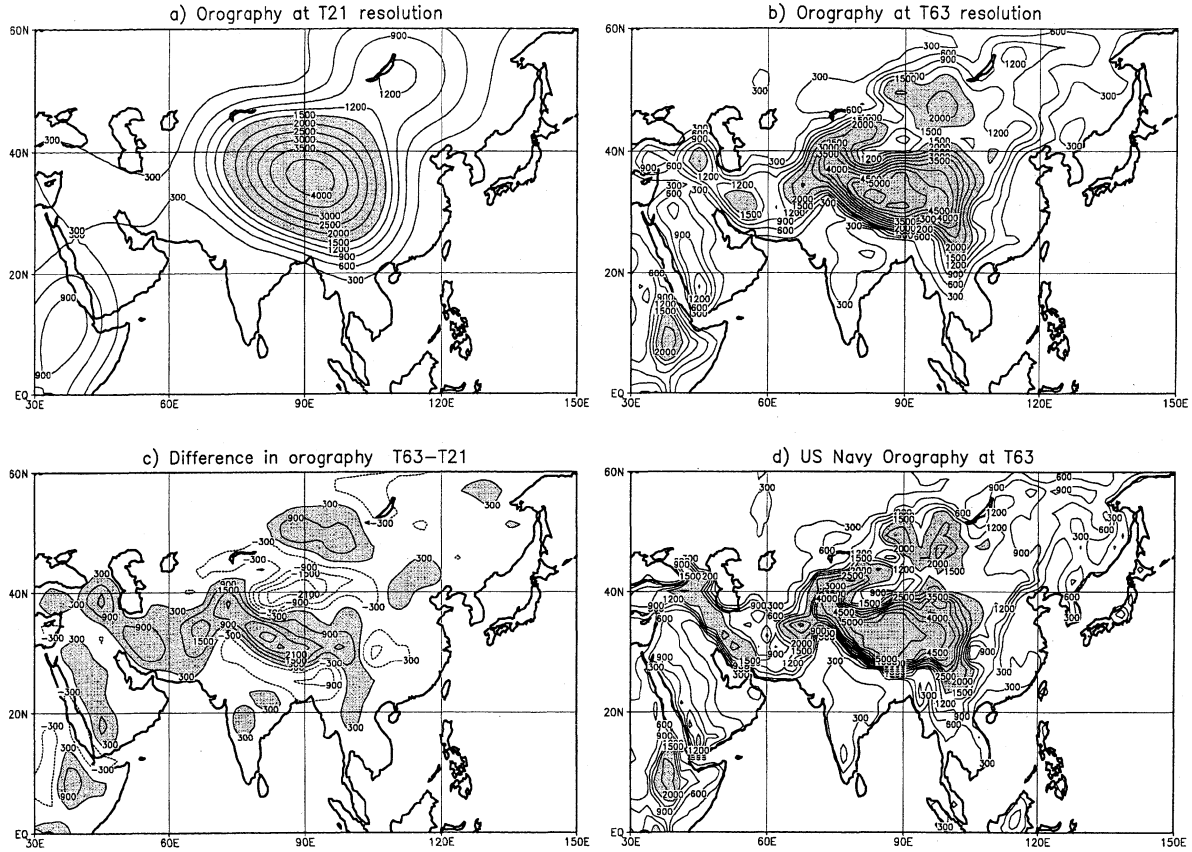


Fig. 7. Representation of Asian monsoon orography: a) at T21 resolution, b) at T63 resolution, c) the difference T63-T21 (contours every 300 m), and d) U.S. Navy orography interpolated by finite differencing to T63 grid. Contours every 300 m below 1500 m, and then every 500 m above 1500 m (shaded).

move realistically southward for resolutions higher than T31.

Asian land surface temperatures in April (not shown) are generally slightly colder at higher resolutions than at lower resolutions with typically about 2°C difference between T21 and T63. The cooling is particularly marked in the Himalayan region, which is more elevated at higher resolutions and has more persistent snow cover. The weakening and southward displacement of the monsoon at higher resolution is consistent with the cooler land surface in springtime. Due to increased precipitation, the initial soil water content is slightly increased at higher resolution and this could explain some of the temperature trend. Work is currently in progress on the surface heat and water budgets.

## 6. Orographic effects

Because of the large differences between the representation of orography at different model horizontal resolutions, and the important role that orography plays in controlling the monsoon, it is likely that some of the changes in the monsoon with model horizontal resolution could be due to changes in the

model orography.

### 6.1 Model representation of orography

In finite numerical models such as GCMs, it is impossible to represent all the details of the orography perfectly, and the orography is usually represented smoothly so as to be consistent with the horizontal resolution of the model. For the ARPEGE model, in which the atmospheric fields are represented as a truncated sum of spherical harmonics, the model orography is obtained by averaging the U.S. Navy 10' global orography onto the model Gaussian grid and then the means are spectrally truncated by Fourier transforming them onto the model spherical harmonics. Examples of the model orography at T21 and T63 resolutions are shown in Fig. 7, together with their difference and the U.S. Navy orography interpolated onto the same grid using the U.S. Navy finite difference interpolation procedures. It can be seen that large differences (not just positive !) exist between the height of the orography at T63 and T21 resolutions and in the steepness of the orography. The elevation of the orography is important in a) causing frictional and barrier effects

in the low level flow (*e.g.*, the East African highlands and the Somali jet), b) cooling the surface temperature by the *lapse rate effect* (Kitoh, 1997), and c) in determining the elevated heat sources produced by latent and sensible surface heating. Steep slopes in the orography cause air packets to uplift and generate vertical motions — the gradient of the slopes is a key factor in controlling vertical velocities and the rate of condensation of saturated air packets. By comparing Fig. 7b and Fig. 7d, it can be seen that coastal orographic features such as the Ghats in southern India and the Burmese mountains have reduced elevation in the T63 model orography. This is due to a variational filtering procedure used to suppress spurious orographic oscillations (Gibbs lobes) in the model orography over oceans, which result from the finite spectral representation of steep orography (Bouteloup, 1995). Such anti-Gibbs filtering is effective in removing unrealistic maxima in simulated precipitation in wet regions such as over the Indian Ocean in the summer monsoon season (Holzer, 1996). However, it can also suppress local maxima in land orography near to the coast unless care is taken to include orographic gradients in the weighting functional as was done in Holzer (1996). This helps to explain why the rain shadow effect of the Ghats only became apparent at T63 resolution, whereas Sperber *et al.* (1994) noticed it at the lower resolution of T42 in studies using the ECMWF spectral model, in which the orography was not filtered to eliminate the oceanic Gibbs lobes.

### 6.2 A smooth mountain experiment: T63s

To estimate the impact of orographic changes on the monsoon when changing the model horizontal resolution, an additional T63 simulation has been performed in which the T63 representation of model orography has been replaced by the smoother orography used in the T21 simulation. This smooth mountain experiment is referred to as T63s and is identical to the previously described T63 simulation, except that it is made with low resolution mountains (globally). The Tibetan plateau is present in T63s but is considerably smoother than at T63 — for example, the southern slopes of the Tibetan plateau have a mean gradient of 3 m/km at T21 (or T63s) resolution compared to 10 m/km at T63 resolution. Hence, the difference between T63s and T63 is not strictly comparable to previous mountain-no mountain studies (Murakami *et al.*, 1970; Hahn and Manabe, 1975; Sadler and Ramage, 1976; and others) but is more comparable to sensitivity studies of mean versus envelope/silhouette orography (WMO 1992, 93; Bhaskar Rao *et al.*, 1991; Fennessy *et al.*, 1994). Silhouette/enhanced orography has steeper slopes and higher peaks because it uses the maximum value in the grid box rather than the mean, and is similar to the envelope orography proposed

by Wallace *et al.* (1983) which adds a fraction of the sub-gridscale standard deviation to the mean orography.

### 6.3 Smooth mountain results

Figure 8 shows the mean JJAS monsoon (1986–1989) obtained for T63s and this can be compared to the observations (Fig. 1) and the other simulations (Figs. 2–5). With the exception of the Himalayan region, the overall precipitation pattern in T63s resembles that obtained for T63, as is confirmed by the area-averaged precipitation (Table 2). In T63s, there is much less excessive precipitation over the southern slopes of the Tibetan plateau, even less than at T21, giving both area-averages and local values in much better agreement with the coarse-gridded observations. The low-level westerly jet (Fig. 8b) is much weaker than in the other simulations — for example, the Somali jet maximum is 14–15 m/s rather than the more realistic 17–18 m/s obtained at the other resolutions. This is most likely related to the reduced height of the East African highlands and a similar reduction has been noted in the idealized mountain studies of Hoskins and Rodwell (1995). The westerly jet is too zonal over India and continues too far eastward into the Southeast Asian peninsula as was the case at lower model resolutions. The excessive zonality is most likely due to insufficient vorticity modification by the suppressed western Ghats and the East African highlands in T63s (Hoskins and Rodwell, 1995). The upper level easterlies (Fig. 8c) are also reduced compared to the other simulations and together with the reduced low-level westerly flow result in a much weaker and more realistic U-index than for the other simulations (Table 3). The weaker and more realistic large-scale monsoon at T63s is also confirmed by the smaller V-index (Table 3) and suggests that the large-scale dynamical monsoon weakens when smoother orography is used in the model. These findings are opposite to those of Bhaskar Rao (1991) and Fennessy *et al.* (1994), who found stronger upper-level easterlies and low-level westerlies in the mean orography case compared to the enhanced orography case. Another noteworthy feature of the T63s simulation is the northward position of the strengthened Tibetan anticyclone (Fig. 8d), reminiscent of the lower resolution simulations (T21 and T31). It is possible that this could be partly due to the steering effect of the northern slopes of the Tibetan plateau which can be seen to extend further north at lower resolution (Fig. 7). More will be said about this in Section 7, which discusses the dynamical effect of the Tibetan plateau.

Figure 9 shows the difference between the T63 simulation and the T63s simulation and can be compared to the T63-T21 difference (Fig. 6), in order to assess the resolution changes due to changes in

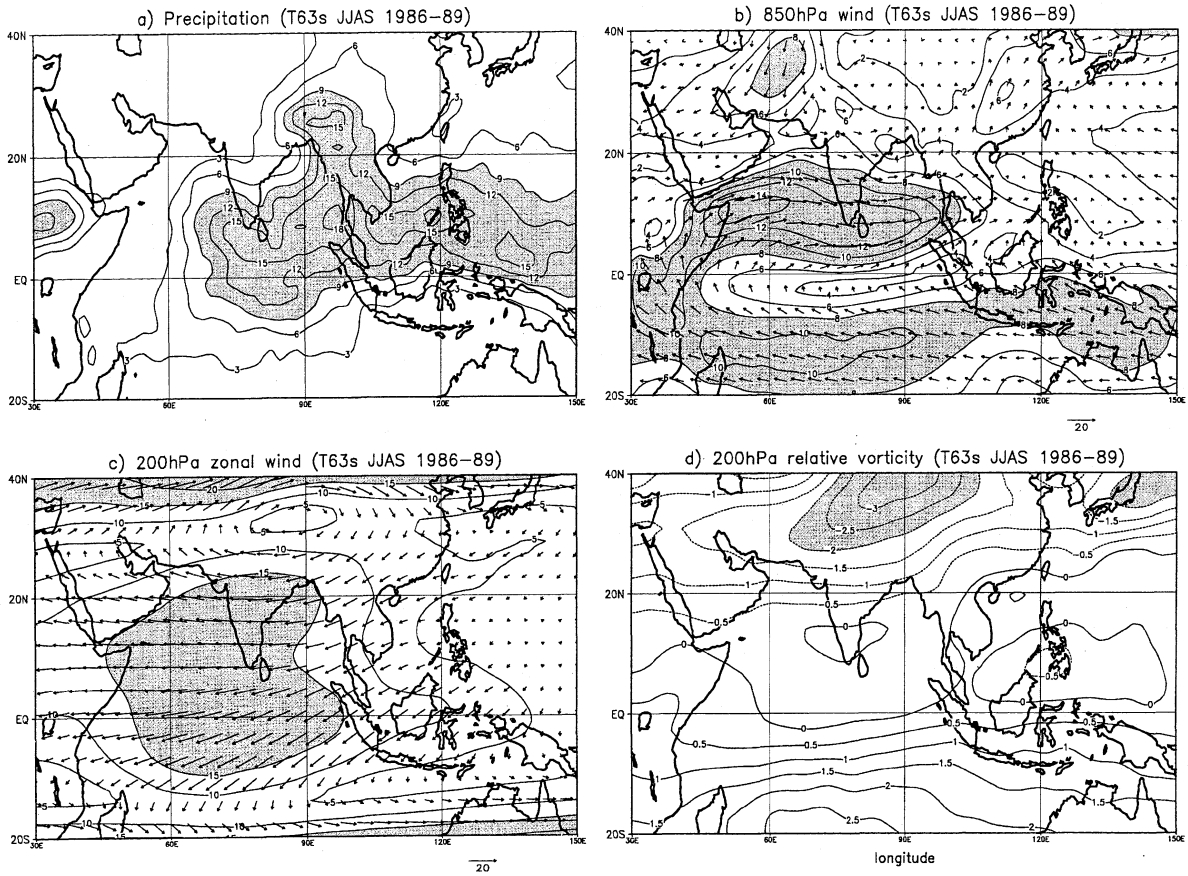


Fig. 8. The mean observed summer monsoon (JJAS) for the smooth orography experiment T63s. a) Mean precipitation rates (contours every 3 mm/day with values above 9 mm/day shaded), b) the mean 850 hPa velocity vectors ( $u, v$ ) and isotachs (every 2 m/s,  $> 8$  m/s shaded), c) the mean 200 hPa velocity vectors ( $u, v$ ) and isotachs (every 5 m/s,  $> 15$  m/s shaded), and d) the mean relative vorticity at 200 hPa (contours every  $0.5 \times 10^{-6} \text{ s}^{-1}$ , and anticyclonic values less than  $-2 \times 10^{-6} \text{ s}^{-1}$  shaded).

the model orography. In general, many of the monsoon changes with resolution, especially those not over land, are not due to the effect of the orography. The increased orography explains the increased precipitation over the Himalayas and northern and central India and the reduced precipitation around 10–15°N over the Bay of Bengal and the Arabian sea. This is in agreement with the results of Bhaskar Rao *et al.* (1991) who found an increase over the Indian sub-continent with enhanced orography, mainly due to enhanced moisture convergence. However, Fennessy *et al.* (1994) found that enhanced orography led to a decrease in precipitation over the entire Indian peninsula by at least 3 mm/day, and ascribed this to dynamically induced changes in the orographically forced stationary waves. It could be that the increased precipitation over India is a local effect due to regionally increased orography, and in general such orography is poorly represented in coarse resolution GCMs. For example, the difference between enhanced and mean orography over India is less than 250 m in Fennessy *et al.* (1994), whereas it exceeds

300 m in T63-T63s. Orography, however, does not explain the large increase in precipitation over the equator and the decrease over the Phillipines. From Fig. 6b, it can be seen that these changes are associated with increased low-level equatorial convergence and decreased convergence over the Phillipines, associated with a general reduction in the westerly jet over Southeast Asia. The orographic effects do not show such a change in the low-level flow but instead show strong changes in the Somalia and Arabia regions (Fig. 9b). With smoother orography, there is less dry air inflow from the Arabian peninsula and Persia. The orography helps to explain upper level flow changes over land (Figs. 6c and 9c) but does not explain the changes in the equatorial easterly flow. Likewise, the change in 200 hPa vorticity over the Asian land mass appears to be due to orographic changes, whereas over the Indian Ocean the orography does not explain all the changes.

To summarize, the T63s smooth mountain simulation is more realistic than the other simulations, in that it has less excessive rainfall over the south-

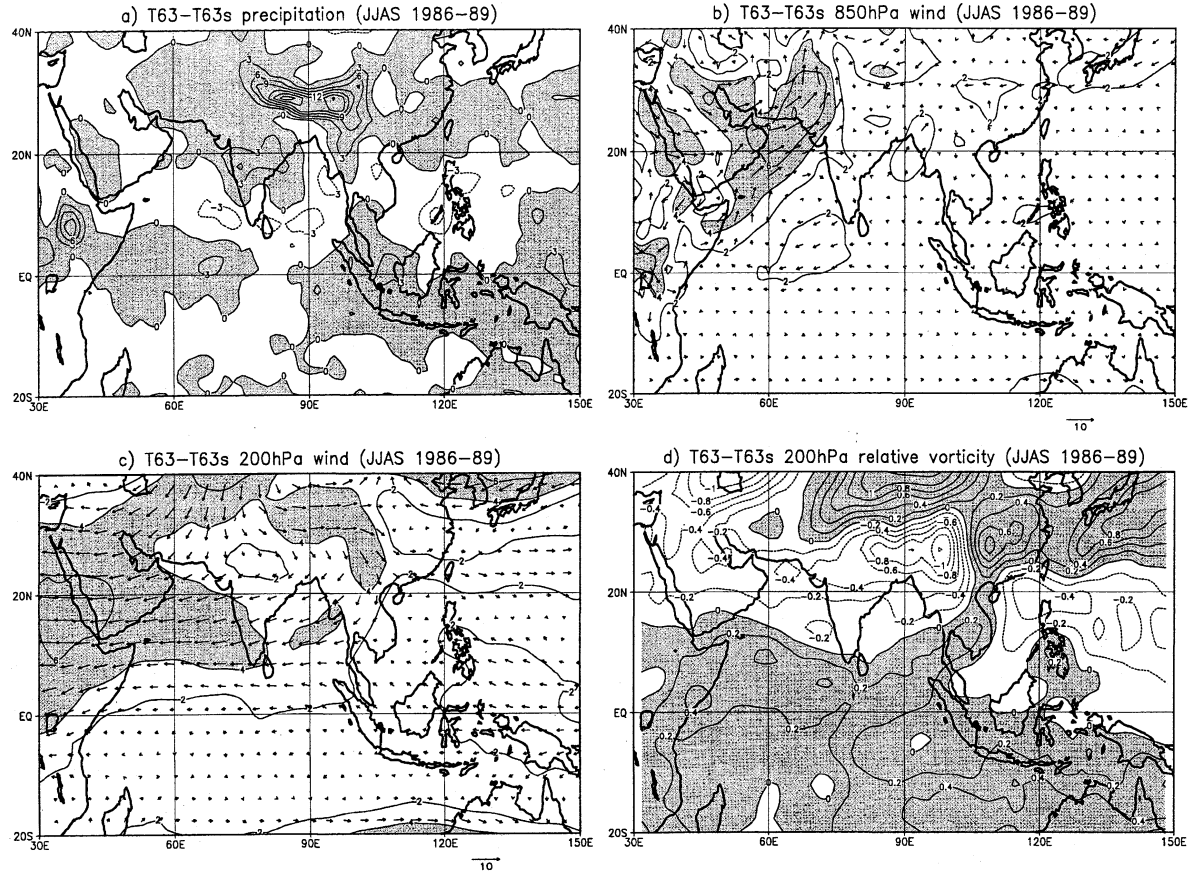


Fig. 9. Mean orographic difference between T63 and T63s summer monsoons (T63-T63s): a) Mean precipitation rates (contours every 3 mm/day with positive values shaded), b) 850 hPa velocity vectors ( $u, v$ ) and isotachs (every 2 m/s,  $> 4$  m/s shaded), c) 200 hPa velocity vectors ( $u, v$ ) and isotachs (every 2 m/s,  $> 4$  m/s shaded), and d) the 200 hPa relative vorticity at 200 hPa (contours every  $0.2 \times 10^{-6} \text{ s}^{-1}$ , and positive values shaded).

ern slopes of the Tibetan plateau, more rainfall over northern India and weaker large-scale shear indices. However, it has a Somali jet which is much too weak and has a Tibetan anticyclone situated too far north compared to ECMWF analyses.

## 7. Dynamical effect of the Tibetan plateau

It has been known for a long time, that the Tibetan (Qinghui-Xizhang) plateau acts as an important heat source for the Asian summer monsoon (Staff Members, Academia Sinica, 1957), and it has even been described as *a heat engine with a giant chimney in its south eastern corner* (Flohn, 1968). Such orography plays a crucial role as an elevated source of mid-tropospheric heating and also in dynamically controlling important features of the monsoon tropospheric flow such as the Tibetan anticyclone. An excellent review of the effects of the Tibetan plateau can be found in Murakami (1987). This section will discuss some of the dynamic effects.

### 7.1 Vertical motions

Yeh and Gao (1979) and Kuo and Qian (1981) presented analyses of the vertical velocities observed over the Tibetan plateau, and these results were confirmed by Luo and Yanai (1983) in their analysis of FGGE observations from late May to early July 1979. In a cross-section at  $92.5^\circ\text{E}$  (their Fig. 12b), in addition to finding intense ascending motion over the Tibetan plateau (with upward velocities exceeding  $-5$  mb/hour), Luo and Yanai (1983) also noted intense ascending motion at 700 hPa over the southern slopes of the Himalayas with a maximum mean upward velocity of  $-4.3$  mb/hour. There was also evidence of strong descent (exceeding 2 mb/hour) at  $(92.5^\circ\text{E}, 42.5^\circ\text{N})$  in the Tarim basin (Tarim Pendi) close to the nuclear test site of Lop Nur. The Tarim basin, sheltered between the Tibetan plateau and the Tien Shan mountains to the north, contains the vast sandy Takla Makan (Taklimakan Shamo), the driest desert in Asia, having dune ridges in its interior rising to elevations of about 100 m above sea-level. In disagreement with previous studies, Luo

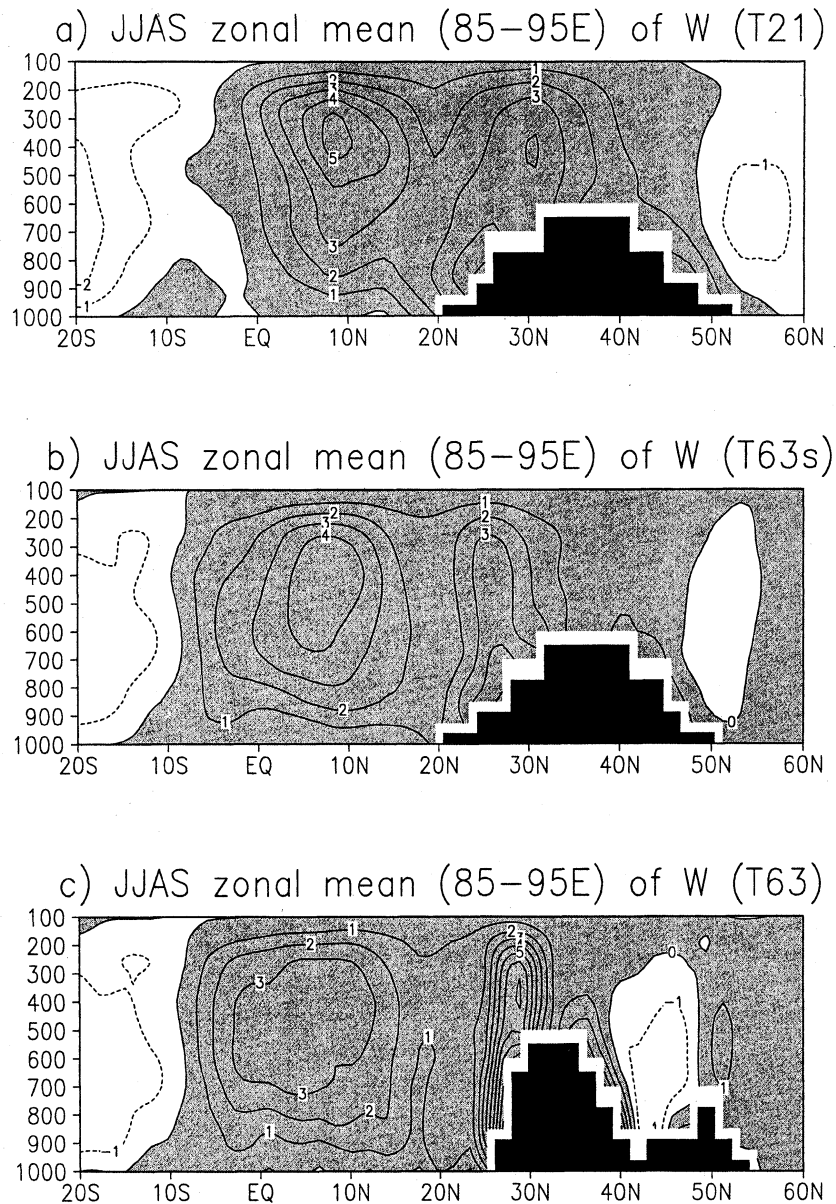


Fig. 10. Latitudinal section of the JJAS mean upward vertical velocity zonally averaged between 85–95°E for a) the T21 experiment, b) the T63 smooth orography experiment, and c) the T63 experiment. Contours every mb/hour and upward values are shaded. Pressures exceeding the mean surface pressure are masked out in black and delineate the Tibetan plateau.

and Yanai (1983) found descending motion at 15°N, which they claimed had also been seen in the model results of Manabe and Hahn (1975). However, the latitudinal cross-section of zonal mean vertical velocity shown in Fig. 4.7 of Manabe and Hahn (1975), reveals upward motion at 15°N, and was described by the authors as one of the *pillars of moist upward motion*. Figure 10 shows a comparable cross-section of the simulated summertime (JJAS) zonally averaged (85–95°E) vertical velocity in units of mb/hour (36 mb/hour = 1 Pa/s). It can be seen that there is marked ascent from EQ–10°N over the

Bay of Bengal and also over the southeastern slopes of the Tibetan plateau. As in Sperber *et al.* (1994), the model fails to create ascent over the top of the plateau, and this may be due to diurnal deficiencies in the land surface parameterisation (Kitoh and Tokioka, 1987). The model simulates latitudinally-confined uplift over the southern slopes of the Tibetan plateau, which increases with resolution to unrealistically large values (more than 7 mb/hour). Also at T63 resolution, the subsidence is simulated over the Tarim basin, and this should be compared to the model results of Sperber *et al.* (1994) who

found that the descent was situated too far north for resolutions less than T106.

### 7.2 Observed Tibetan anticyclone vorticity budget

One of the prominent features of the Asian monsoon is the development of a strong upper tropospheric anticyclone over the Tibetan plateau. The anticyclone is clearly visible as a strong negative minimum in upper tropospheric relative vorticity, as seen in Figs. 1d and Fig. 5, and represents a major perturbation in the upper tropospheric tropical circulation. In order to understand the dynamics of the monsoon flow, it is of interest to ask what mechanisms are responsible for the formation and maintenance of the Tibetan anticyclone. One possible explanation was given by Krishnamurti (1971a, b) who suggested that the upper level divergence associated with ascending air parcels could act as a source for anticyclonic relative vorticity,  $\partial_t \zeta = -\zeta_a \nabla \cdot \mathbf{u}$ , caused by the vertical stretching of the air parcels. Air parcels forced to rise by either a) underlying orography, and/or b) convective heating, become compressed in the upper tropospheric outflow regions and in the Northern Hemisphere this can then act as a source of anticyclonic relative vorticity. Steering of the westerly jet around the northern side of the plateau would cause the air packets to rise over the topography and would give rise to vertical compression of air packets on the northern side of the plateau. Stretching/compression of air packets also occurs to the south of the plateau due to ascent caused by monsoon convection. Both these processes could contribute to the generation of anticyclonic vorticity at upper levels.

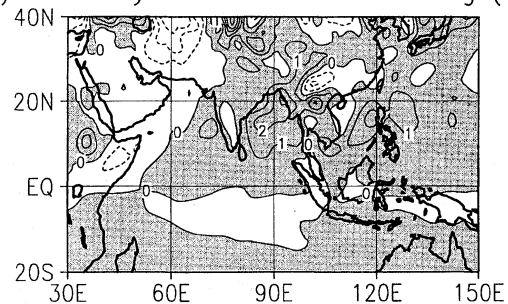
Sardeshmukh and Hoskins (1985) showed that the major large-scale upper level tropical vorticity dynamics is contained in the equation

$$\frac{\partial \zeta}{\partial t} = -\zeta_a \nabla \cdot \mathbf{u} - \mathbf{u} \cdot \nabla \zeta_a + \epsilon \quad (1)$$

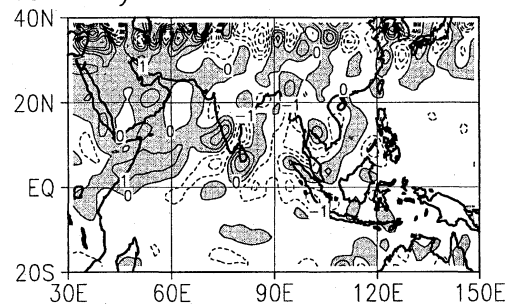
where  $\zeta$  and  $\zeta_a$  are the relative and absolute vorticity, respectively, and  $\epsilon$  refers to small residual terms associated with vertical advection/twisting, and dissipation. The first term on the right hand side is due to *vertical stretching* and the second term is due to *horizontal advection* of absolute vorticity. Sardeshmukh and Hoskins (1985) also noted that in the time-mean balance, *transients play a small though not insignificant role* in the time mean residual term. It should also be noted that the horizontal advection term is non-linear and is not simply due to meridional advection of the planetary vorticity gradient ( $\beta v$ ), as is often assumed in simplified tropical heating models (Gill, 1980).

Although Sardeshmukh and Held (1984) performed a detailed analysis of the vorticity budget using GCM results and found that there was *considerable cancellation between the stretching and horizontal advection by the time mean flow in the vicinity*

a) Tendency from vertical stretching (ERA)



b) Tendency from horizontal advection (ERA)



c) Total tendency from a) and b) (ERA)

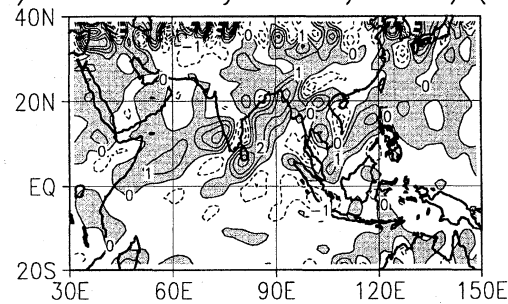


Fig. 11. 200 hPa mean relative vorticity tendencies for the T106 ECMWF re-analyses JJAS 1985–1989, from a) mean vertical stretching ( $\zeta_a \nabla \cdot \mathbf{u}$ , and b) mean horizontal advection ( $\mathbf{u} \cdot \nabla \zeta_a$ ). Contours every  $10^{-10} \text{ s}^{-2}$  with anticyclonic positive tendencies shaded. The tendencies have been smoothed slightly using a 9-point stencil (smth9 in GrADS) to make them more readable.

of the Tibetan anticyclone, there have been no studies of the monsoon vorticity budget using observed analyses of the atmosphere. To remedy this deficit, Fig. 11 shows the time-mean stretching and horizontal advection tendencies for the ECMWF JJAS analyses for the period 1986–89. The stretching term shows upper-level divergence features associated with the precipitation maxima over the Bay of

Bengal and off the west coast of India. Although there are quite a lot of small-scale features, especially in the advection term, it can be seen that in general the large-scale patterns do not cancel one another. The sum of the two terms equals the divergence of the mean absolute vorticity flux,  $\nabla \cdot (\bar{u} \bar{\zeta}_a)$ , and can be seen to differ significantly from zero (Fig. 11c). There are net contributions from the horizontal advection term over southern India and the Bay of Bengal, and a net anticyclonic tendency from the stretching term over the north of India and the Tibetan plateau. Since the time-mean of the vorticity tendency over 3 months is negligible, the sum of the time-mean stretching and horizontal advection tendencies must be balanced by the time-mean of the residual terms caused by vertical advection/twisting, transient vorticity fluxes and dissipation terms. The residual terms can only be accurately calculated by accumulating the terms obtained at each time step of the reanalysis integrations, and these were unfortunately not available. It may be possible that the ECMWF parameterisation of vertical cumulus mixing of horizontal momentum (*cumulus friction*) could be playing a role in the vorticity budget in the vertically sheared monsoon region (Moncrieff and Klinker, 1997). A detailed budget study of the ECMWF and NCEP six-hourly reanalyses, similar to the GCM analysis of Sareshmukh and Held (1984), could help answer such questions. Holton and Colton (1972) found that they could reproduce the 200 hPa rotational flow by making the crude assumption that the time-mean residual terms act as a form of vorticity damping, in other words,  $\bar{\epsilon} \approx -r\bar{\zeta}$ , where  $r$  is a damping coefficient of the order of 1/day. Using this simple linear model, Held and Sardeshmukh (1984) were capable of obtaining a rough approximation of the model's Tibetan anticyclone given the time-mean stretching and horizontal advection vorticity tendencies.

### 7.3 Modelled Tibetan anticyclone vorticity budget

Large differences between different model resolutions have already been presented for the 200 hPa relative vorticity, the most noteworthy being the tendency of the Tibetan anticyclone to move southwards at higher resolution. It is of interest to relate these changes to those seen in the large-scale ascent, by examining the tendency terms contributing to the upper level vorticity budget. Figure 12 shows the stretching and advection terms for the T63 and T63s model results. An unrealistically large unbalanced anticyclonic tendency occurs in the stretching terms over the southern slopes of the Tibetan plateau. It is much less in T63s compared to that in T63 in consistent agreement with the reduced orographic precipitation already noted in T63s.

The strong anticyclonic tendency is balanced to

some extent over China and South East Asia by a strong cyclonic horizontal advection tendency. It remains, however, unbalanced over the Tibetan plateau, which may explain why the Tibetan anticyclone became centered further south over Tibet at higher resolution. From Fig. 12, it appears that unlike the ECMWF analyses which show large amounts of stretching over the Bay of Bengal, most of the stretching is occurring further north over the southern slopes of the Tibetan plateau, associated with the excessive convection. A much smaller contribution is visible on the northern slopes of the plateau, which suggests that the steering effect of the plateau may play less of a role in determining the anticyclone than does the convection to the south. The unrealistic cyclonic horizontal advection tendency over China and Southeast Asia is due to a strong southward flow in the model, advecting the meridional gradient in absolute vorticity, thereby acting so as to cancel the anticyclonic stretching tendency in these regions. Such a meridional flow is obscured to a large extent by the zonal component when making plots of the 200 hPa wind velocity vectors. By careful comparison, however, of Figs. 2e and 4e in Ju and Slingo (1995), excessive southward flow can be discerned in the model results and it is of interest to remark that this model also suffered from excessive precipitation over the southern slopes of the Tibetan plateau. The strong meridional flow transports dry upper-level air towards the southern hemisphere and contributes to an overly active upper branch in the local Hadley circulation, as seen in the large values of V-index. It is encouraging to note that the model appears to be capturing some of the regional features over the Bay of Bengal such as the anticyclonic tendency due to the advection term.

Assuming that the time-mean residual term acts as a form of vorticity damping, a possible explanation for why the Tibetan anticyclone moves southward with increased resolution is that the anticyclonic vorticity tendency increases due to the increased vertical compression associated with the excessive convection over the southern slopes of the Tibetan plateau. A possible reason why the Tibetan anticyclone is too far north in the smooth orography experiment T63s, having more realistic Tibetan rainfall, is that the model misses the rainfall maximum observed over the head of the Bay of Bengal, which from Fig. 11a can be seen to play a substantial role in the upper tropospheric vorticity budget. It should be noted that the vorticity damping coefficient can have spatial variations, and these may modulate the response so that spatial features in the net vorticity tendency no longer coincide with the resulting features in the vorticity response.

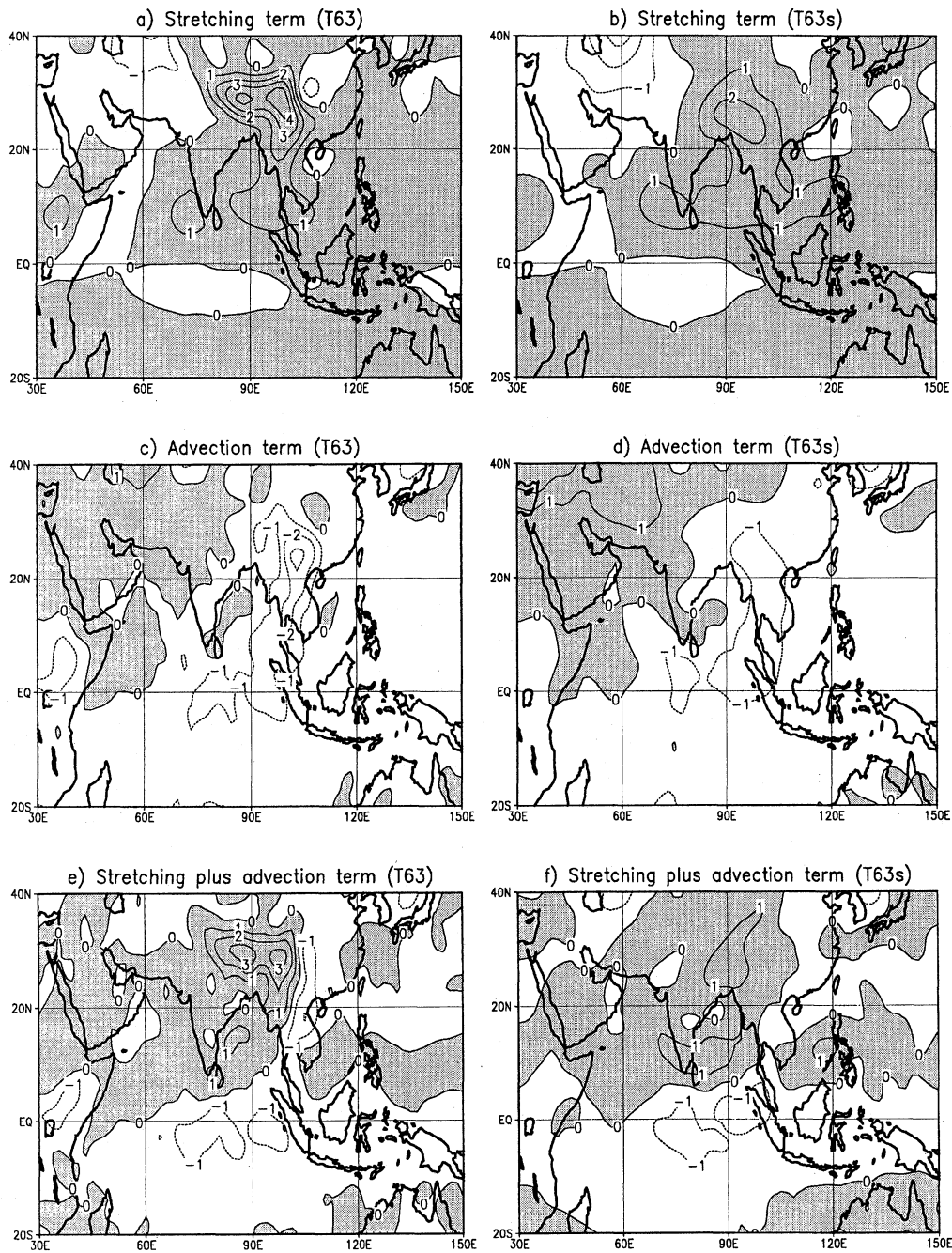


Fig. 12. 200 hPa mean relative vorticity tendencies due to a) mean vertical stretching in the T63 experiment, b) mean vertical stretching in the T63s experiment, c) mean horizontal advection in the T63 experiment, and d) mean horizontal advection in the T63s experiment. Contours every  $10^{-11} \text{ s}^{-2}$  with anticyclonic positive tendencies shaded. The fields have been smoothed slightly using a 9-point stencil (smth9 in GrADS) to reduce the small-scale noisiness.

## 8. Intensification of the equatorial convergence

The smooth orography test has demonstrated that many of the resolution changes over land can be explained by associated changes in the representation of orography. However, many differences can still be seen between the results of the T63s and

T21 experiments (Fig. 13), which both had identical T21 orography. It is instructive to decompose the total difference T63-T21 (Fig. 6) into the sum of the orographic difference T63-T63s (Fig. 9) and the residual difference T63s-T21 (Fig. 13). Most of the large-scale patterns in T63-T21, not adjacent to the Tibetan plateau, are also found in the residual T63s-T21, and hence can not be attributed to

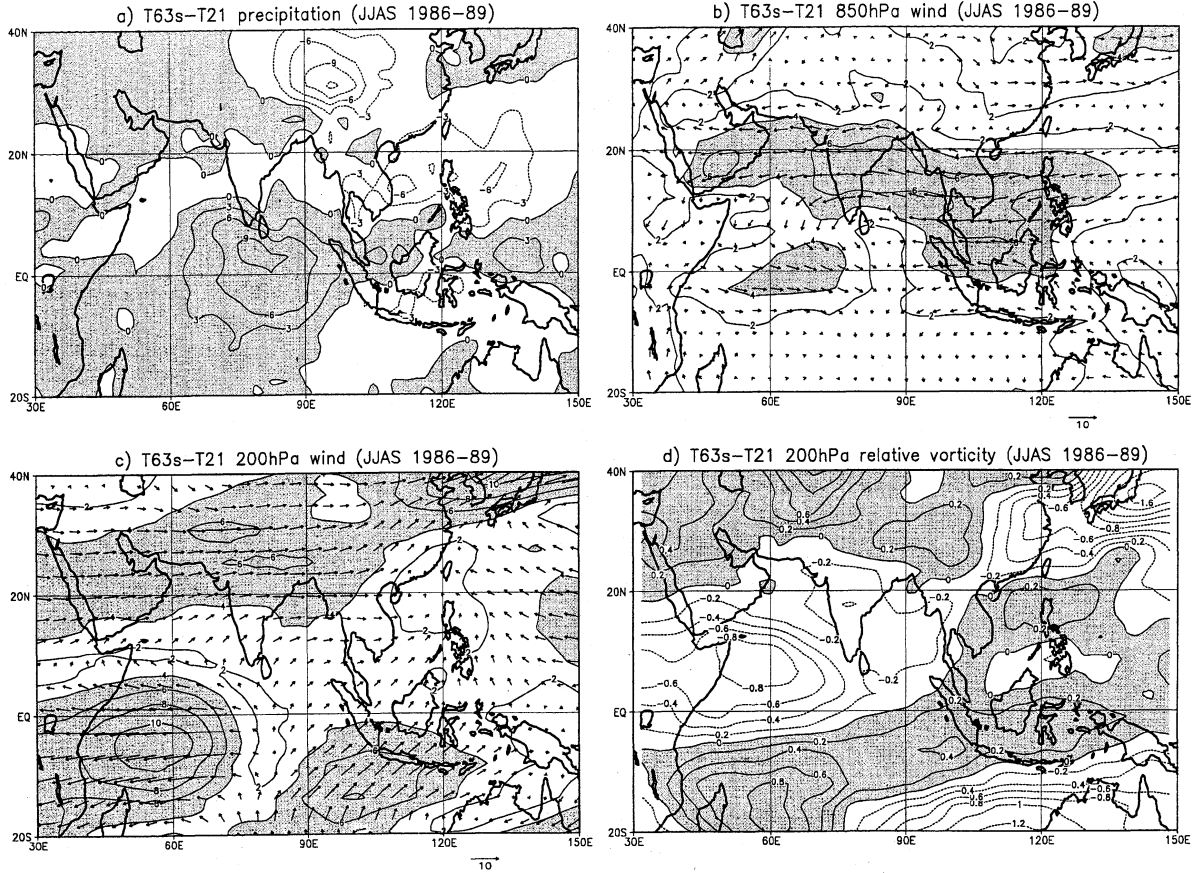


Fig. 13. Mean non-orographic residual difference between T63s and T21 summer monsoons (T63s-T21):  
 a) Mean precipitation rates (contours every 3 mm/day with positive values shaded), b) 850 hPa velocity vectors ( $u, v$ ) and isotachs (every 2 m/s,  $> 4$  m/s shaded), c) 200 hPa velocity vectors ( $u, v$ ) and isotachs (every 2 m/s,  $> 4$  m/s shaded), and d) the 200 hPa relative vorticity at 200 hPa (contours every  $0.2 \times 10^{-6} \text{ s}^{-1}$ , and positive values shaded).

changes in the orographic representation. In T63-T21, there is a marked increase in precipitation over the equatorial Indian Ocean and a decrease over the Tibetan plateau, China and the Phillipines, which is not explainable by changes in orography. Despite the difficulties of how to discern causality in a complex non-linear climate system, it is tempting to ask the question: What could have caused these non-orographic differences?

A possible response to this question comes from the behaviour of the modelled equatorial convergence zones with resolution. Stephenson and Royer (1995) noted in their study of the simulated Southern Oscillation using a previous version of the ARPEGE model, that the equatorial convergence intensified with increased model resolution, especially in the eastern equatorial Pacific. The same effect also occurs in the model simulations presented in this article, as is evident in Fig. 14 which shows the summertime mean outgoing longwave radiation — a much-used proxy for convective activity. The Pacific and Atlantic convergence zones clearly be-

come narrower and intensify with increasing model resolution, causing the difference between T63 and T21 (not shown) to increase in the zones and decrease north and south of them. Typical T63-T21 differences are of the order of  $40 \text{ W.m}^{-2}$  and decreased convection occurs between the latitudes of  $10\text{--}35^\circ\text{N}$  over the Pacific and Asian sectors. The trend in the convergence zones in the tropical Pacific and Atlantic becomes apparent even in the second month of the simulations (April), before the onset of the monsoon (not shown). In the Indian ocean sector, the equatorial OLR increases with increasing resolution, and this causes the OLR maximum to become situated further southwest, consistent with the large scale changes seen in the rainfall distribution. The Indian Ocean convergence zone extends south of the equator and the increased OLR at T63 occurs between the equator and  $10^\circ\text{S}$ , slightly south of the increase previously noted in the precipitation.

The model parameterizes sub-grid scale cumulus convective processes using the Bougeault (1985) mass-flux scheme. As the model grid becomes finer,

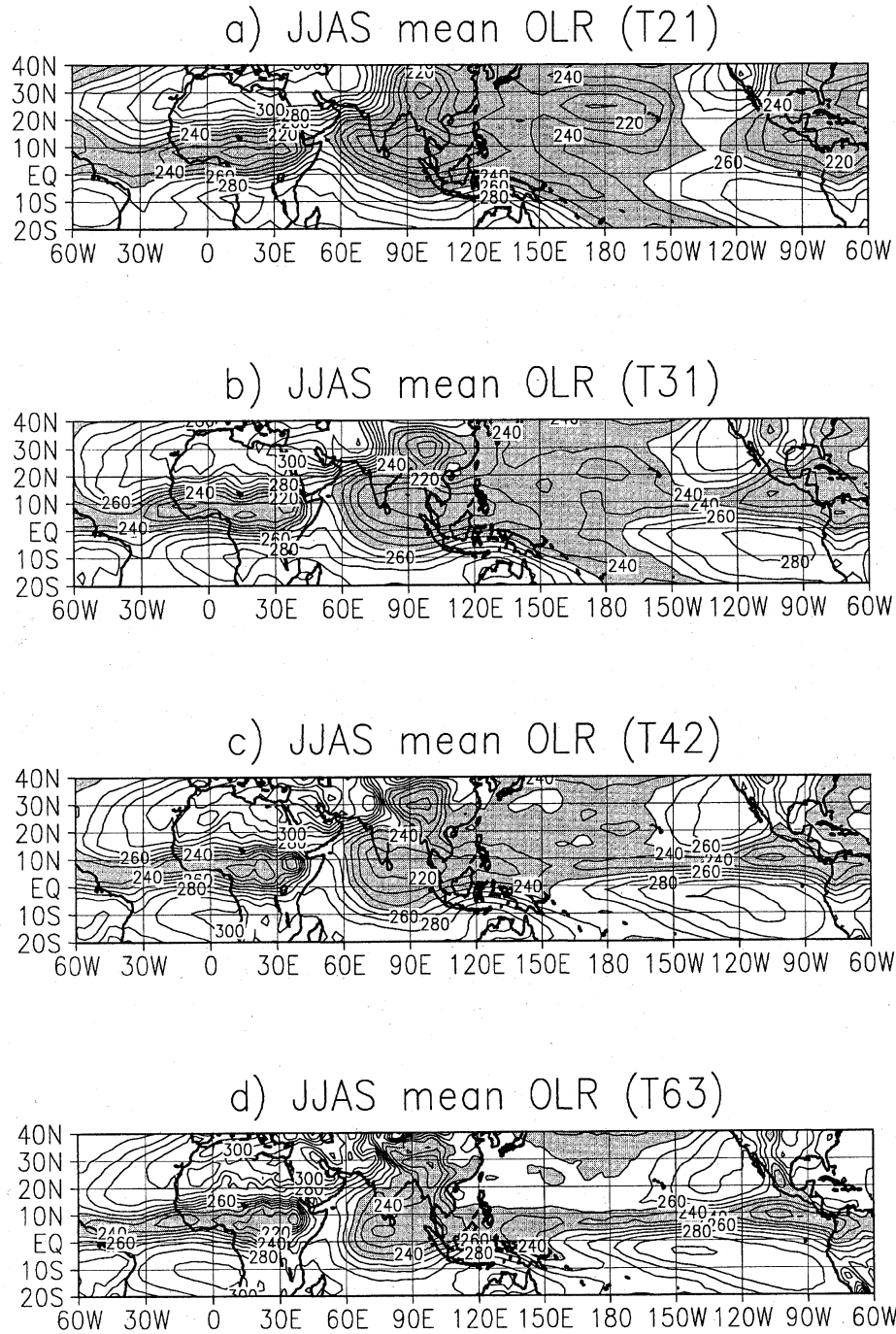


Fig. 14. Mean JJAS outgoing longwave radiation for the a) T21, b) T31, c) T42, and d) T63 experiments. Contours every  $10 \text{ W}\cdot\text{m}^{-2}$  with shading for cloudy regions having values less than  $250 \text{ W}\cdot\text{m}^{-2}$ .

local circulations become simulated explicitly by the model and there is less need for their implicit parameterization. Furthermore, mesoscale tests have revealed that at increased resolution, the model simulates increased amounts of precipitation (Bougeault and Geleyn, 1989). This led Chen and Bougeault (1993a) to modify the convection scheme by introducing a scaling factor to relate the rate of moisture convergence to the large-scale vertical moisture

advection. This resolution-dependent factor can be considered as a mesoscale dynamic parameter accounting for more efficient mesoscale circulations within larger grid boxes (Krishnamurti *et al.*, 1983). Chen and Bougeault (1993b) found an empirical dependence on resolution by demanding that the total rainfall remained the same at the three different resolutions of 40, 80 and 160 km. An empirical scaling has also been incorporated into the ARPEGE op-

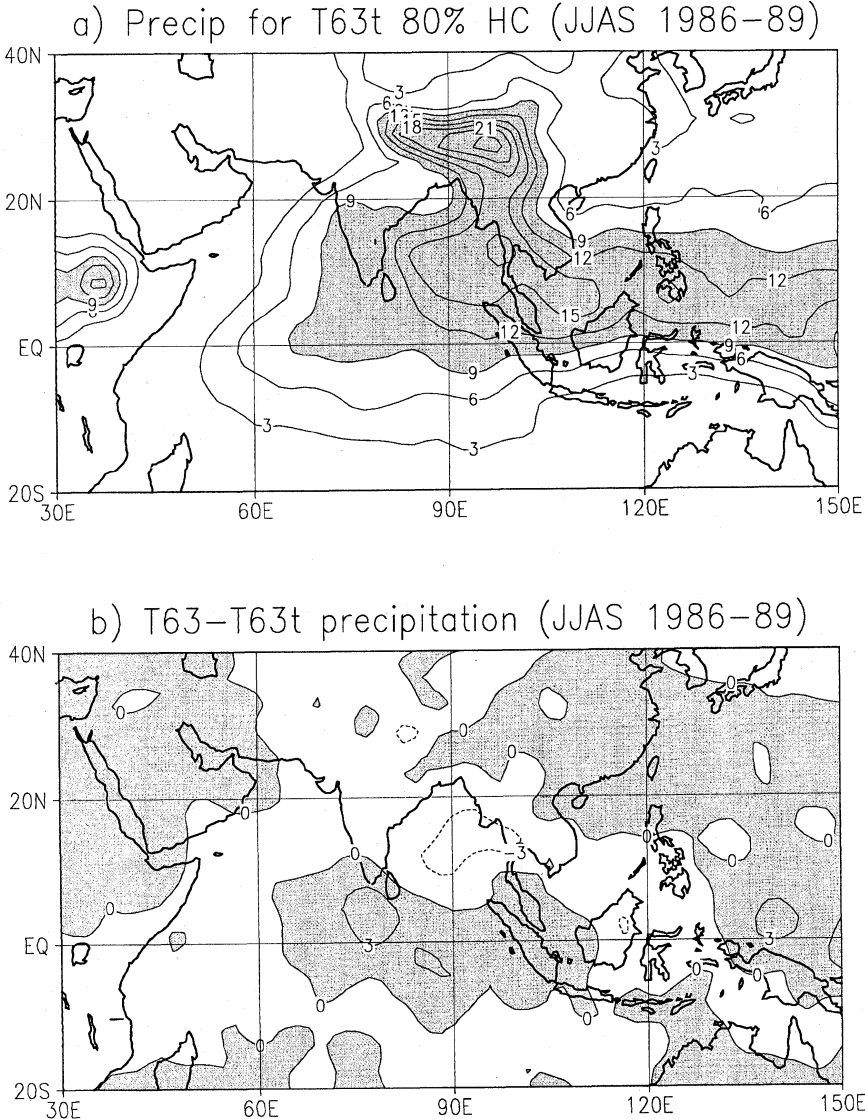


Fig. 15. a) Mean JJAS precipitation for the T63t experiment having 0.8 of the humidity horizontal convergence supplied to the convection scheme, and b) The difference between the control experiment T63 and T63t (contours every 3 mm/day and positive values shaded).

erational forecasting model and is useful for avoiding excessive precipitation in the stretched grid version of the model (J-F. Geleyn, personal communication).

#### 8.1 A reduced convergence experiment: T63t

In the current simulations, resolution-dependent limitation of the humidity supplied to the convection scheme was not activated, and explains why the convergence zones intensify with increasing resolution. It is of interest, therefore, to reduce the supplied humidity convergence at high resolution in order to reduce the intensity of the convergence zones, and thereby see their influence on the monsoon. An additional T63 simulation has been performed for the years 1986–1989 with the horizontal moisture convergence supplied to the convection scheme multi-

plied by a reduction factor of 0.8. The resulting mean JJAS precipitation for this experiment, T63t, is shown in Fig. 15a, and the difference with the control simulation (T63–T63t) is presented in Fig. 15b. Reducing the moisture convergence supplied to the convective parameterization closure, has limited the excessive mean precipitation in the convergence zone over the equatorial Indian Ocean. It has also helped to increase, realistically, the amount of precipitation over the Bay of Bengal, which was perhaps suppressed by compensating subsidence induced by the excessive equatorial convergence zone. Compared to the T63 values quoted in Table 2, there is less mean precipitation over the EQU region (9.8 mm/day) and more mean precipitation over the EXT region (10.7 mm/day). Hence, the intensification of the convergence zones with resolution may explain some

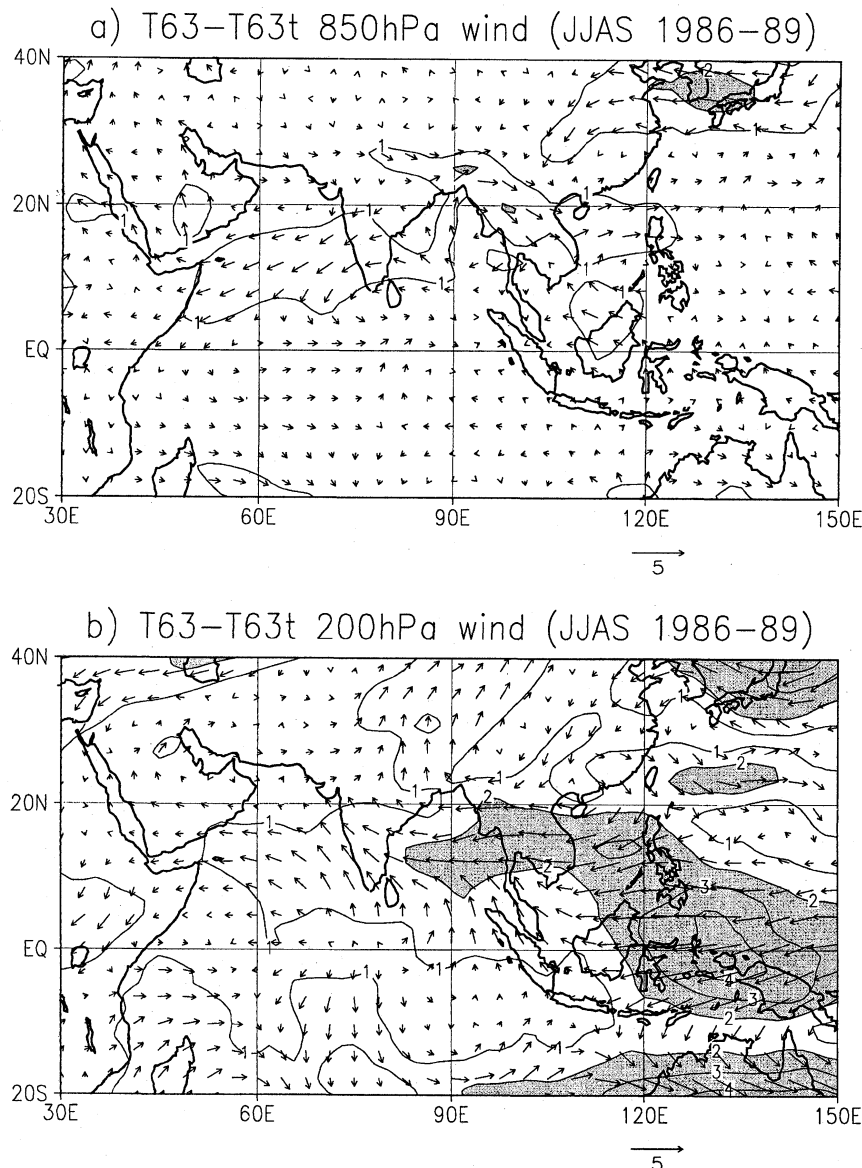


Fig. 16. Dynamical impact of reducing the moisture convergence supplied to the convection scheme. The T63-T63t difference in a) the 850 hPa flow, and b) the 200 hPa flow. Note that the isotachs are every 1 m/s and are half those in previous difference figures.

of the resolution trends in the precipitation.

It is astonishing to note that such non-negligible changes in convective activity, have overall very little effect on the monsoon dynamical circulation at 850 and 200 hPa — differences are shown in Fig. 16 (note the scales are half that in previous figures). In multiplying the humidity convergence by a factor of 0.8, the U-index decreases by only 0.1 from 25.8 and the V-index decreases from 6.2 by only 0.1. There has been practically no impact on the large-scale zonal and meridional monsoon circulations. The reduction in convection is centered on the equatorial Indian Ocean and does not have a large meridional scale, and hence such equatorial vertical stretching is not likely to induce a large vorticity source in the upper troposphere. From sim-

ple vorticity arguments, off-equatorial convection is expected to have a much larger impact on the rotational part of the flow, and it is this effect which dominates the large-scale mean monsoon flow. This convection test has shown that the excessive equatorial precipitation maximum can be reduced by tuning down the humidity convergence supplied to the convection scheme, yet without having a strong impact on the dynamics of the monsoon circulation. Such a weak coupling between the model dynamics and the equatorial convection also provides an explanation for why many GCMs can have excessive equatorial precipitation in the Indian Ocean while also having reasonable off-equatorial monsoon circulations (e.g., Ju and Slingo, 1995).

## 9. Concluding remarks

A comparison has been made of the mean Asian summer monsoons simulated by the ARPEGE GCM with spectral truncations from 21–63 total wavenumbers, corresponding to model horizontal resolutions ranging from 600–200 km. Due to the Asian monsoon having many different phenomenological aspects, it is a difficult task to summarize the resolution behaviour, yet such an exercise is of use in assessing the relative merits of running at higher and more computationally costly resolutions.

Some simulated features become more realistic with increasing resolution. Perhaps the most noteworthy are the changes in the low-level westerly jet. At low resolutions, the jet has a tendency to continue too far eastward and has a jet core centered too far north and east of Somalia. As the resolution is increased, these systematic errors diminish and at T63 the Findlater jet core is correctly situated near to Somalia. Unlike the studies of Tibaldi *et al.* (1990) and Sperber *et al.* (1994), there is no discernible differences in the maximum jet speed with resolution. The westward contraction of the westerly jet also has the effect of reducing the dynamic large-scale monsoon U-index towards more realistic values. Furthermore, a similar beneficial reduction trend is seen in the meridional V-index suggesting that the local monsoon Hadley circulation also becomes more realistic at higher resolution.

Unfortunately, not all features improve with increased resolution and some model systematic errors become worse at high resolution. For example, at all resolutions the model has excessive precipitation over the southern slopes of the Tibetan plateau, which is a problem common to many GCM simulations. Whereas the excessive area-average total precipitation over the slopes (the HIM index) generally increases by only a small amount with resolution (10.5 mm/day at T21 compared to 11.8 mm/day at T63), the local values increase dramatically due to the precipitation being concentrated into a narrower region on steeper slopes. The enhanced topography mainly contributes to spatially redistributing the total precipitation into a narrower band as was also discussed by Giorgi and Marinucci (1996). This leads to large local rainfall rates and excessive vertical motions at high resolution. Another systematic error of the model which becomes worse at higher resolutions is the excessive precipitation over the equatorial Indian Ocean. This is also an error common to many GCM monsoon simulations and was seen to get worse when ARPEGE was coupled to a global ocean model (Stephenson, 1995).

Previous modelling studies have shown that the mountainous orography in Asia and East Africa can have a controlling effect on the Asian monsoon. Furthermore, the representation of orography becomes

much more realistic as resolution is increased. For example, the gradient of the southern slope of the Tibetan plateau increases by about a factor of three in going from T21 to T63 resolution. Hence, it is of interest to ask which of the resolution changes are attributable to changes in the orographic representation. To answer this question, we have performed a *smooth* orography experiment in which we prescribed low resolution orography in a high resolution GCM. This experiment shows much less precipitation over the southern slopes of the Tibetan plateau and much more realistic dynamic large-scale monsoon indices. There is also less ascent over the slopes and less vertical stretching which can generate anticyclonic relative vorticity. Perhaps as a result of this lack of vorticity tendency, the Tibetan anticyclone becomes situated north of the plateau as also occurs at lower resolutions. The smooth orography also gives reduced precipitation over northern and central India as observed at lower resolutions, and hence the increase of this with resolution is most likely due to the increased elevation of local orography. Further south, at 10°N over the ocean, the precipitation decreases with resolution and this effect is not seen when comparing the smooth mountain experiment with lower resolution results. It is possible that this southerly band of decreased precipitation is partly due to the suppression of convection by subsiding air coming from the enhanced convection over the southern slopes of the Tibetan plateau. Increased precipitation over the northern foothills of India and the slopes of the Himalayan mountains and reduced precipitation over the south of India and the surrounding ocean is one of the signatures of a monsoon *break* episode. Hence, it is tempting to summarize the monsoon changes over India by saying that the model is more in a *break* mode than an *active* mode as resolution increases. However, this appealing bimodal concept is perhaps too simplified to explain all the details. It is known that many convective monsoon systems are steered around the foothills of the Himalayas and the mountains of Burma and tests are in progress to see what effect drag and lift forces have on steering such systems.

Although the changes in orography explain some of the changes related to resolution, they by no means explain all the differences (or even the majority). There is a systematic trend for low-level equatorial convergence to intensify as resolution is increased. This effect can be reduced by limiting the moisture convergence supplied to the cumulus convection parameterisation. A test has been performed at T63 resolution, with the moisture convergence reduced by 20 %. The test has the effect of reducing the excessive precipitation over the equatorial Indian Ocean with very little impact on the dynamical monsoon flow. Hence, the non-orographic

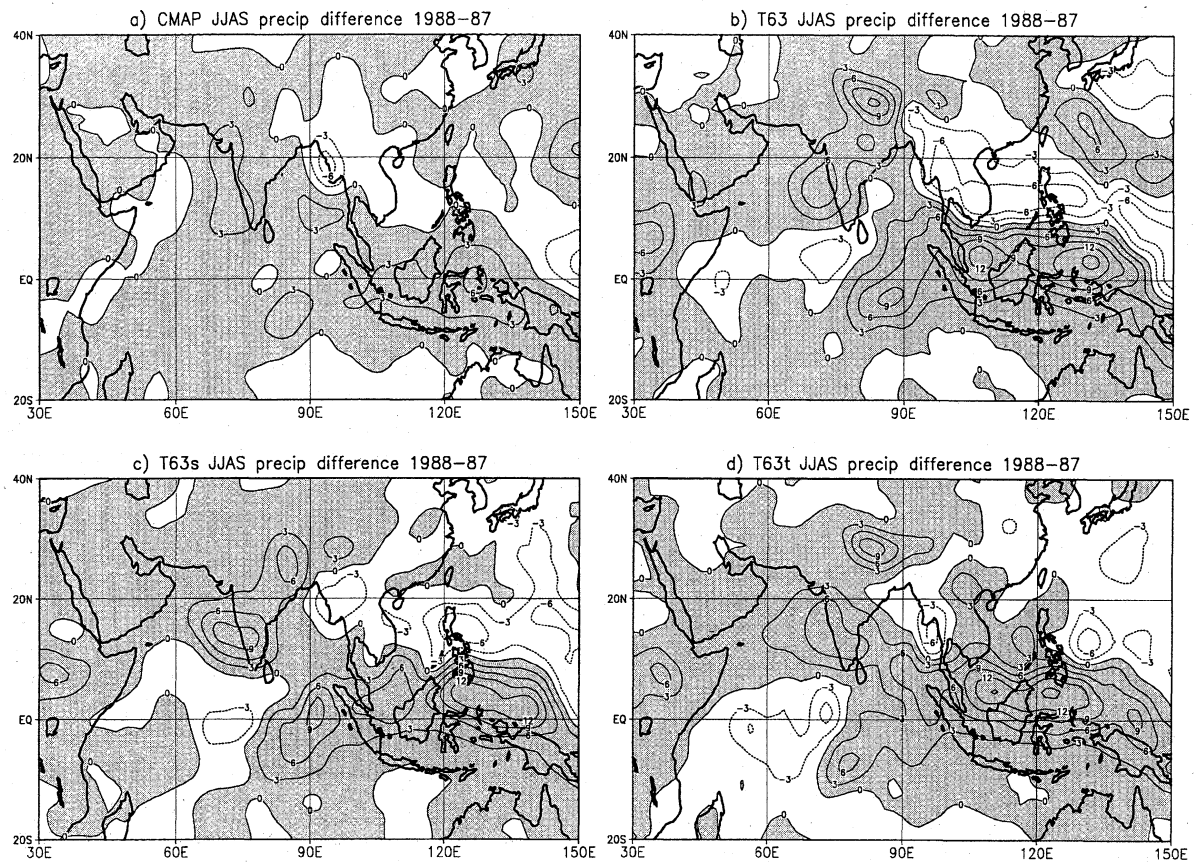


Fig. 17. Mean JJAS precipitation differences between the years 1988–1987 for a) the CMAP observations, b) the T63 simulation, c) the T63s smooth orography simulation, and d) the T63t reduced convection simulation. Contours are every 3 mm/day with negative values shaded.

changes with resolution can not be solely attributed to the intensification of the mean convergence zones, and it is likely that changes in transient behaviour also play a role.

It is of historical interest to note that Gilchrist (1977) concluded his intercomparison of four different model simulations of the monsoon by saying that the simulation of more detailed characteristics, particularly the rainfall distributions, *leave a great deal to be desired*. He also concluded that *many of the shortcomings seem to be most evident near mountains*. Many of the systematic errors presented in his intercomparison study still dominate current attempts to successfully model the Asian summer monsoon, as has been demonstrated in this study. It is unfortunate that many of these errors do not simply ameliorate by increasing the model horizontal resolution, and many even become worse. On a more optimistic note, preliminary studies at T63 of the 1987 and 1988 precipitation patterns reveal that despite the mean state being sensitive to orographic representation and convective parameterizations, the interannual variations are relatively insensitive to these changes in the mean monsoon rainfall distribution (Fig. 17). This interesting result could

be specific to the strongly anomalous 1987 and 1988 monsoons and is currently under more detailed investigation. Because of its intrinsic complexity, the realistic simulation and understanding of the Asian monsoon and its variability are likely to remain major challenges for many years to come.

#### Acknowledgments

David Stephenson thanks Klaus Arpe, Hervé Douville, B.N. Goswami, Brian Hoskins, Katia Laval, Virginie Lorant, Akio Kitoh, K. Rupa Kumar, Jerry Meehl, Julia Slingo, and Ken Sperber for their helpful scientific remarks. Thanks also go to Phil Arkin, Ping Ping Xie, Mike Hulme and the U.S. Navy personnel at Diego Garcia for their assistance with the observed Indian Ocean rainfall data. The figures in this article were prepared using the graphics software GrADS, with the kind help of Brian Doty and Mike Fiorino, and the assistance of Charles Doutriau who supplied the U.S. Navy orography data. Finally, we wish to thank Michel Déqué at Météo-France for his help in answering innumerable technical questions concerning the modus operandi of the GCM. This study was supported by a Framework IV

grant (ENV4-CT95-0122) from the European Commission as part of the SHIVA monsoon project.

## References

- Bhaskar Rao, D.V., K. Yamazaki and A. Kitoh, 1991. Some GCM experiments of the Asian summer monsoon related to land boundary conditions. *Pap. Meteor. Geophys.*, **42**, (3), 127–143.
- Bhaskaran, B., R.G. Jones, J.M. Murphy, and M. Noguer, 1996. Simulations of the Indian summer monsoon using a nested regional climate model: Domain size experiments. *Clim. Dyn.*, **12**, (9), 573–587.
- Boer, G.J. and M. Lazare, 1988. Some results concerning the effect of horizontal resolution and gravity wave drag on simulated climate. *J. Climate*, **1**, (8), 789–806.
- Bougeault, P., 1985. A simple parameterization of the large-scale effects of cumulus convection. *Mon. Wea. Rev.*, **113**, 2108–2121.
- Bougeault, P. and J-F. Geleyn, 1989. Some problems of closure assumption and scale dependency in the parameterization of moist deep convection for numerical weather prediction. *Meteor. Atmos. Phys.*, **40**, 123–135.
- Bouteloup, Y., 1995. Improvement of the Spectral Representation of the Earth Topography with a Variational Method. *Mon. Wea. Rev.*, **123**, 1560–1573.
- Boville, B.A., 1991. Sensitivity of simulated climate to model resolution. *J. Climate*, **4**, (5), 469–485.
- Boyle, J.S., 1993. Sensitivity of dynamical quantities to horizontal resolution for a climate simulation using the ECMWF (cycle 33) model. *J. Climate*, **6**, (5), 796–815.
- Chen, D. and P. Bougeault, 1993a. A simple prognostic closure assumption to deep convective parametrization: Part I. *Acta Meteorologica Sinica*, **7**, 1–18.
- Chen, D. and P. Bougeault, 1993b. A simple prognostic closure assumption to deep convective parametrization: Part II. *Acta Meteorologica Sinica*, **7**, 212–223.
- Chen, Tsing-C. and J.J. Tribbia, 1993. An effect of the model's horizontal resolution on stationary eddies simulated by the NCAR CCM1. *J. Climate*, **6**, (8), 1657–1664.
- Déqué, M., C. Dreveton, A. Braun and D. Cariolle, 1994. The ARPEGE/IFS atmosphere model: A contribution to the French Community climate modelling. *Clim. Dyn.*, **10**, 249–266.
- Déqué, and J-P. Piedelievre, 1995. High resolution climate simulation over Europe. *Clim. Dyn.*, **11**, 321–339.
- Doblas-Reyes, F.J., M. Déqué, D.B. Stephenson and F. Valero, 1998. North-Atlantic Wintertime Intraseasonal Variability and its Sensitivity to GCM Horizontal Resolution. *Accepted for publication in Tellus*.
- Dong, B., P.J. Valdes and N.M.J. Hall, 1996. The changes of Monsoonal Climates due to Earth's Orbital Perturbations and Ice Age Boundary Conditions. *Paleoclimates*, **1**, 203–240.
- Douville, H. and J.F. Royer, 1996. Sensitivity of the Asian summer monsoon to an anomalous Eurasian snow cover within the Météo-France GCM. *Clim. Dyn.*, **12**, (7), 449–446.
- Douville, H. and J.F. Royer and J-F. Mahfouf, 1995a. A new snow parameterisation for the Météo-France climate model, Part I: Validation in stand-alone experiments. *Clim. Dyn.*, **12**, 21–35.
- Douville, H. and J.F. Royer and J-F. Mahfouf, 1995b. A new snow parameterisation for the Météo-France climate model, Part I: Validation in a 3D GCM experiment. *Clim. Dyn.*, **12**, 37–52.
- Fennelly, M.J., III Kinter, J.L., B. Kirtman, L. Marx, S. Nigam, E. Schneider, J. Shukla, D. Straus, A. Vernekar, Y. Xue and J. Zhou, 1994. The simulated Indian monsoon: A GCM sensitivity study. *J. Climate*, **7**, (1), 33–43.
- Findlater, J., 1969. A major low-level air current near the Indian Ocean during the northern summer. *Quart. J. Roy. Meteor. Soc.*, **95**, (404), 362–380.
- Flohn, H., 1968. Contributions to a meteorology of the Tibetan Highlands. *Atmospheric science Paper No. 130, Department of Atmospheric Science, Colorado State University, Fort Collins*, **130**.
- Gadgil, S., S. Sajani and participating modelling groups of AMIP, 1998. Monsoon precipitation in the AMIP runs. *WMO-WCRP Technical Report*, (in press).
- Geleyn, J.F., E. Bazile, P. Bougeault, M. Déqué, V. Ivanovici, A. Joly, L. Labb  , J.P. Piedelievre, J.M. Piriou and J.F. Royer, 1995. Atmospheric parameterization schemes in M  t  o-France's ARPEGE NWP model. *ECMWF Seminar: Parameterization of Sub-grid Scale Physical Processes*, 385–402.
- Gibson, J.K., P. K  llberg, A. Nomura and S. Uppala, 1994. The ECMWF Re-Analysis (ERA) project — plans and current status. *ECMWF Workshop Proc.: Fourth Workshop on Meteorological Operational Systems, 22–26 November 1993*, 162–169.
- Gilchrist, A., 1977. The simulation of the Asian summer monsoon by general circulation models. *Pure Appl. Geophys.*, **115**, (5/6), 1431–1448.
- Gill, A.E., 1980. Some simple solutions for heat-induced tropical circulation. *Quart. J. Roy. Meteor. Soc.*, **106**, (449), 447–462.
- Giorgi, F. and M.R. Marinucci, 1996. An investigation of sensitivity of simulated precipitation to model resolution and its implications for climate studies. *Mon. Wea. Rev.*, **124**, (1), 148–166.
- Gleckler, P.J. and K.E. Taylor, 1993. The effect of horizontal resolution on ocean surface heat fluxes in the ECMWF model. *Clim. Dyn.*, **9**, (1), 17–32.
- Goswami, B.N., V. Krishnamurthy and H. Annamalai, 1997. A Broad Scale Circulation Index for Interannual Variability of the Indian Summer Monsoon. *Submitted to QJRMS*.
- Hahn, D.G. and S. Manabe, 1975. The role of mountains in the South Asian monsoon circulation. *J. Atmos. Sci.*, **32**, 1515–1541.
- Halton, J.R. and D.E. Colton, 1972. A diagnostic study of the vorticity balance at 200 mb in the tropics during northern summer. *J. Atmos. Sci.*, **29**, 1124–1128.
- Holzer, M., 1996. Optimal spectral topography and its effect on model climate. *J. Climate*, **9**, (10), 2443–2463.
- Hoskins, B.J. and M.J. Rodwell, 1995. A model of the Asian summer monsoon. Part I: The global scale. *J. Atmos. Sci.*, **52**, (9), 1329–1340.

- Ju, J. and J. Slingo, 1995. The Asian summer monsoon and ENSO. *Quart. J. Roy. Meteor. Soc.*, **21**, 1133–1168.
- Kar, S.C., M. Sugi and N. Sato, 1996. Simulation of the Indian summer monsoon and its variability using the JMA Global model. *Pap. Meteor. Geophys.*, **47**, (2), 65–101.
- Kiehl, J.T. and D.L. Williamson, 1991. Dependence of cloud amount of horizontal resolution in the National Center for Atmospheric Research Community Climate Model. *J. Geophys. Res. Atmos.*, **96**, (6), 10955–10980.
- Kitoh, A., 1997. Mountain uplift and surface temperature changes. *Geophys. Res. Lett.*, **24**, 185–188.
- Kitoh, A. and T. Tokioka, 1987. A Simulation of the Tropospheric General Circulation with the MRI Atmospheric General Circulation Model Part III: The Asian Summer Monsoon. *J. Meteor. Soc. Japan*, **65**, 167–186.
- Kitoh, A., S. Yukimoto, A. Noda and T. Motoi, 1997. Simulated Changes in the Asian Summer Monsoon at Times of Increased Atmospheric CO<sub>2</sub>. *J. Meteor. Soc. Japan*, **75**, 1019–1031.
- Krishnamurti, T.N., 1971a. Tropical east–west circulations during the Northern summer. *J. Atmos. Sci.*, **28**, (8), 1342–1347.
- Krishnamurti, T.N., 1971b. Observational Study of the Tropical Upper Tropospheric Motion Field during the Northern Hemisphere Summer. *J. Appl. Meteor.*, **10**, 1066–1096.
- Krishnamurti, T.N., S. Low-Nam and R. Pasch, 1983. Cumulus parameterization and rainfall rates II. *Mon. Wea. Rev.*, **111**, 816–828.
- Kuo, H.L. and Y.F. Qian, 1981. Influence of the Tibetan Plateau on cumulative and diurnal changes of weather and climate in summer. *Mon. Wea. Rev.*, **109**, 2337–2356.
- Lal, M., U. Cubasch, J. Perlitz and J. Waszkewitz, 1997. Simulation of the Indian monsoon climatology in ECHAM3 climate model: Sensitivity to horizontal resolution. *Intl. J. Climatol.*, **17**, 847–858.
- Legates, D.R. and C.J. Willmott, 1990. Mean seasonal and spatial variability in gauge-corrected, global precipitation. *Intl. J. Climatol.*, **10**, (2), 111–127.
- Luo, H. and M. Yanai, 1983. The large-scale circulation and heat sources over the Tibetan Plateau and surrounding areas during the early summer of 1979. Part I: Precipitation and kinematic analyses. *Mon. Wea. Rev.*, **111**, (5), 922–944.
- Mahfouf, J-F., A.O. Manzi, J. Noilhan, H. Giordani and M. Déqué, 1995. The land surface scheme ISBA within the Météo-France climate model ARPEGE. Part I: Implementation and preliminary results. *J. Climate*, **8**, 2039–2057.
- Moncrieff, M.W. and E. Klinker, 1997. Organised convective systems in the tropical western Pacific as a process in general circulation models: A TOGA COARE case-study. *Quart. J. Roy. Meteor. Soc.*, **123**, 805–827.
- Murakami, T., 1987. Effects of the Tibetan Plateau. *Monsoon Meteorology*, pages 235–270. Oxford University Press, New York.
- Murakami, T., R.V. Godbole and R.R. Kelker, 1970. Numerical simulation of the monsoon along 80°E. *Proceedings of the conference on the summer monsoon in South East Asia*, ed. C.S. Ramge, 39–51.
- Noilhan, J. and S. Planton, 1989. A simple parameterization of land surface processes for meteorological models. *Mon. Wea. Rev.*, **117**, 536–549.
- Pant, G.B. and K. Rupa Kumar, 1997. *Climates of South Asia*. John Wiley & Sons Ltd.
- Reynolds, R.W. and T.M. Smith, 1994. Improved global sea surface temperature analyses using Optimum Interpolation. *J. Climate*, **7**, (6), 929–948.
- Rodwell, M.J. and B.J. Hoskins, 1995. A model of the Asian summer monsoon. Part II. Cross-equatorial flow and PV behavior. *J. Atmos. Sci.*, **52**, (9), 1341–1356.
- Royer, J.F., M. Déqué and F. Chauvin, 1994. Monsoon circulations and variability in 10 year simulations with a GCM at different resolutions. *Proceedings of the International Conference on Monsoon variability and prediction (Trieste, Italy, 9–13 May 1994)*. WCRP-84 (WMO/TD), **619**, pp 702–709.
- Sadler, J.C. and C.S. Ramage, 1976. Comments on “The role of mountains in the South Asian monsoon circulation. *J. Atmos. Sci.*, **33**, 2255–2262.
- Sardeshmukh, P.D. and I.M. Held, 1984. The vorticity balance in the tropical upper troposphere of a general circulation model. *J. Atmos. Sci.*, **41**, 768–778.
- Sardeshmukh, P.D. and B.J. Hoskins, 1985. Vorticity balances in the tropics during the 1982–83 El Niño–Southern Oscillation event. *Quart. J. Roy. Meteor. Soc.*, **111**, (468), 261–278.
- Shukla, J. and M. Fennessy, 1994. Simulation and Predictability of Monsoons. *Proceedings of International Conference on Monsoon variability and prediction (Trieste, Italy, 9–13 May 1994)*, WCRP-84 (WMO/TD), **619**, pp 567–575.
- Sperber, K.R., S. Hameed, G.L. Potter and J.S. Boyle, 1994. Simulation of northern summer monsoon in the ECMWF model: Sensitivity to Horizontal Resolution. *Mon. Wea. Rev.*, **122**, 2416–2481.
- Sperber, K.R. and T.N. Palmer, 1961. Interannual tropical rainfall variability in general circulation model simulations associated with the Atmospheric Model Intercomparison Project. *J. Climate*, **9**, 2727–2750.
- Staff Members, Academia Sinica, 1957. On the general circulation over Eastern Asia (I). *Tellus*, **9**, 432–446.
- Stephenson, D.B., 1994. The impact of changing the horizontal diffusion scheme on the northern winter climatology of a general circulation model. *Quart. J. Roy. Meteor. Soc.*, **120**, 1–16.
- Stephenson, D.B., 1995. The Asian Monsoon in a globally coupled ocean atmosphere circulation model. *Proceedings of the Second International Study Conference on GEWEX in Asia and GAME (Pattaya, Thailand, 6–10 March 1995)*. pp 184–187.
- Stephenson, D.B. and J.F. Royer, 1995. GCM simulation of the Southern Oscillation from 1979–88. *Clim. Dyn.*, **11**, (2), 115–128.
- Tibaldi, S., Plamer, T.N., C. Brankovic and U. Cubasch, 1990. Extended-range predictions with ECMWF models: Influence of horizontal resolution on systematic error and forecast skill. *Quart. J. Roy. Meteor.*

- Soc.*, **116**, 835–866.
- Wallace, J.M., S. Tibaldi and A.J. Simmons, 1983. Reduction of systematic forecast errors in the ECMWF model through the introduction of envelope orography. *Quart. J. Roy. Meteor. Soc.*, **109**, (462), 683–718.
- Webster, P.J. and S. Yang, 1992. Monsoon and ENSO: Selectively interactive systems. *Quart. J. Roy. Meteor. Soc.*, **118**, 877–926.
- Williamson, D.L., J.T. Kiehl and J.J. Hack, 1995. Climate sensitivity of the NCAR Community Climate Model (CCM2) to horizontal resolution. *Clim. Dyn.*, **11**, (7), 377–379.
- WMO, 1992. Simulation of interannual and intraseas-
- onal monsoon variability. WCRP-68, WMO/TD, **470**, Geneva, Switzerland.
- WMO, 1993. Simulation of prediction of monsoon recent results. WCRP-68, WMO/TD, **546**, Geneva, Switzerland.
- Xie, P., P.A. Arkin, 1996. Analyses of global monthly precipitation using gauge observation, satellite estimates, and numerical model predictions. *J. Climate*, **9**, 840–858.
- Yeh, T.-C and Y.-X. Gao, 1979. The Meteorology of the Qinghai-Xizang (Tibet) plateau. *Science Press, Beijing*, 278 pp. (in Chinese).
- Zwiers, F.W., 1994. Some aspects of climate intercomparison, *NCAR Technical Note TN-409*, 67–70.

## アジアの夏のモンスーンのシミュレーションとモデルの水平解像度への依存性

David B. Stephenson · Fabrice Chauvin · Jean-François Royer

(Météo-France CNRM, 42 Avenue Gaspard Coirolis, 31057 Toulouse Cedex, France)

1986 ~ 1989 年のアジアの夏のモンスーンを、全波数 63, 42, 31, 21 で波数切断した、水平解像度 200 ~ 600 km 相当の、最新の大気大循環モデルを用いてシミュレートした。7 ~ 9 月平均のアジアモンスーンを解析し、観測された平均的なモンスーンの振舞と比較した。対流圏下層の西風ジェット、熱帯対流圏上層の東風、チベット高気圧、アジア大陸の夥しい降水量などの大規模な特徴は、すべての解像度のモデルで再現される。解像度を上げるにつれて、下層西風ジェットのコアがソマリアの方向に移動し、より現実的なる。しかし、赤道インド洋とチベット高原南斜面で降水量が多すぎ、これらの誤差は解像度を上げるとより大きくなる。さらに、解像度モデルではチベット高気圧の位置が南偏することに明瞭に現れるように、モンスーン域が南に移動する。上層の渦度収支の解析から、これはチベット高原の南斜面で上昇流が強すぎることと関係していることが示唆される。地形の寄与を評価するために、波数 21 で切断した地形で波数 63 のモデルを走らせることによって、平滑化された地形をテストした。平滑化された地形は、チベット高原南斜面の過度の降水量を軽減し、陸上のモンスーンに強くかつ一般に有益なインパクトを与える。それによってまた、大規模な力学的なモンスーンの指標が観測とより一致するようになるが、赤道インド洋の過度の降水量は軽減されない。海上の過度の降水量は、幾分かは、解像度を上げると赤道域の収束帶が系統的に強化するためであるが、それはモンスーン循環の力学とは弱くしか結合していないように見える。